A Coupled Resonator Reflex Klystron*

By E. D. REED

(Manuscript received March 5, 1953)

The theory of a coupled resonator reflex klystron is developed and its reduction to practice described. This tube differs from the conventional reflex klystron in that its performance characteristic is derived from the interaction between the electronic admittance due to a bunched electron stream and the input admittance of two synchronously tuned, coupled resonators. As a result: (1) power output can be made to be substantially flat over the greater part of the electronic tuning range; (2) the half-power electronic tuning range of the coupled resonator reflex klystron is more than twice that of a klystron using the same electron optical system but interacting with a single resonator; and (3) modulation linearity may be obtained over a greatly increased frequency swing.

A reduction in power output of about 3db occurs for a secondary resonator Q and coupling coefficient adjustment designed to yield a maximum flat band or maximum electronic tuning while a much smaller reduction in output power will provide a substantial improvement in modulation linearity.

TABLE OF CONTENTS

* Submitted in partial fulfillment of the requirements for the degree of Doctor of Philosophy, in the Faculty of Pure Science of Columbia University.

1.0 INTRODUCTION

The conventional reflex klystron derives its performance characteristics from the interaction between the electronic admittance due to a bunched electron stream and the input admittance of a resonant cavity. As is well known, this interaction results in mode shapes which are closely related to certain input properties of the passive resonant circuit. Thus, the dependence of power output upon frquency, which results from variations in repeller voltage about its mid-mode value, bears close resemblance to the input-impedance-versus-frequency plot of a parallel resonant circuit. Similarly, the curve relating frequency to repeller voltage has the same general shape as that relating frequency to the input phase angle of the resonator. Recognition of these relationships has resulted in the consideration of different and, perhaps, more useful mode shapes which might be obtained if the electronic admittance were made to interact with impedance or admittance functions of passive circuits other than that due to a single resonator.

What do we mean by "more useful" mode shapes? The answer, of course, depends on the application, although an "ideal" mode shape could probably be defined as one having a flat top, i.e., power output inde-

pendent of repeller voltage, with frequency linearly related to the latter. Moreover, these conditions should preferably obtain over the widest possible frequency range. A tube possessing such characteristics would prove exceedingly useful in a large number of applications. To list a few:

(a) Electronically swept signal generator,

(b) FM deviator,

(c) Transmitting oscillator in radio relay systems employing frequency modulation, and

(d) Local oscillator in microwave receivers with wide range AFC applied to the repeller.

Inability to realize this ideal mode shape in a practical tube might make a compromise solution appear acceptable, one consisting of a reflex klystron having a variable mode shape, i.e., a characteristic which could be adjusted to fit a particular need. Thus, application (a) requires constant power output with minor emphasis on frequency-repeller-voltage linearity, whereas applications (b) and (c) demand a high degree of modulation linearity with constancy of power output of no great importance. In application (d) the emphasis is on wide electronic tuning with both variation in power output and non-linearity in the frequency characteristic permissible.

A method to obtain this variable mode shape was achieved by the use of coupled cavities. Instead of having the bunched electron stream interact with the electric field of a single resonator, as is done in the conventional reflex klystron, we can present to it the input admittance of two coupled cavities. The resultant mode shape may then be expected to resemble the input impedance of two coupled resonant circuits just as the conventional klystron mode resembles that of a single resonator. Moreover, the input impedance of two coupled cavities can assume a large variety of contours depending on the ratio of Q's of the primary and secondary resonators and on the tightness of coupling between the two. If we were now to construct such a double cavity reflex klystron with provision to vary the secondary Q as well as the coupling coefficient continuously, we would have the means of producing a large variety of mode shapes within a single tube. Depending on the application, the characteristics could then be adjusted to give either a range of flat power output or optimum modulation linearity or wide electronic tuning.

As might be expected at this point, a price must be paid for the advantages gained in the coupled cavity approach. It consists of the power expended in supplying the losses due to the secondary resonator. This power subtracts directly from the available useful power and, there-

fore, though resulting in broadband operation, greatly improved modulation linearity and a number of other useful properties, leads to a definite reduction in output level. Whether this can be tolerated will again depend on the application. In many practical cases the performance flexibility inherent in the coupled resonator reflex klystron will more than outweigh this advantage.

It is the purpose of this paper to present the theory underlying the operation of the coupled resonator reflex klystron, as well as its experimental verification. For the sake of completeness, but also in order to emphasize methods of analysis to be used in later sections and not readily found in the literature, a review of reflex klystron theory will precede the exposition of the coupled resonator problem. In both the single and coupled resonator case, performance analysis will be based on a separate and independent study of the electronic and passive circuit admittance developed across the interaction gap and upon the graphical combination of the two in the complex admittance plane. As a by-product of this investigation, a number of driving point properties of two coupled resonant circuits will be developed which may be found of general networks interest. Following the theory of the coupled resonator reflex klystron, an experimental tube of this type will be described and a qualitative as well as quantitative verification of the theory given. Oscillograms will be presented showing the advantages of this device when used as a sweep generator, both in the microwave band and at lower frequencies. Additional applications will be indicated in the hope that others may try them.

2.0 SMALL SIGNAL REFLEX KLYSTRON THEORY

This section will be devoted to a brief review of the small signal reflex klystron theory. Emphasis will be on concepts leading to the equivalent circuit representation and to the graphical admittance-plane analysis. Both of these and particularly the graphical approach will later be used in the investigation of coupled cavity behavior.

As stated before, the operation of the reflex klystron is the result of the interaction between a bunched electron stream and the varying electric field existing inside a resonant cavity. In circuit language, this amounts to an interaction between an active and a passive element. The active one due to the electron stream is termed electronic admittance, and the passive one is the input admittance of the resonator. Derivations for the expression describing the electronic admittance may be readily found in the literature.[1] It will not be repeated here. The re-

sult of these derivations, however, and its physical significance will be discussed at some length.

2.1 *Electronic Admittance*

Consider an arrangement of four plane and parallel elements consisting of a cathode, two ideal grids and a reflector. Assume these electrodes to be of infinite extent so that all electrons will move in straight paths perpendicular to the planes of the electrodes. Let the current densities encountered be low enough so that space charge effects can be neglected. Both grids are operated at the same dc potential, V_0, positive with respect to the cathode. As shown in Fig. 1, this might be achieved by connecting them to the secondary winding of an ideal transformer having a 1:1 turns ratio. The reflector is operated at a dc potential, V_R, negative with respect to the cathode. Next, an RF voltage of amplitude V is applied to the transformer and, hence, appears across the grids. Electrons emitted from the cathode are accelerated toward the first grid and arrive at it

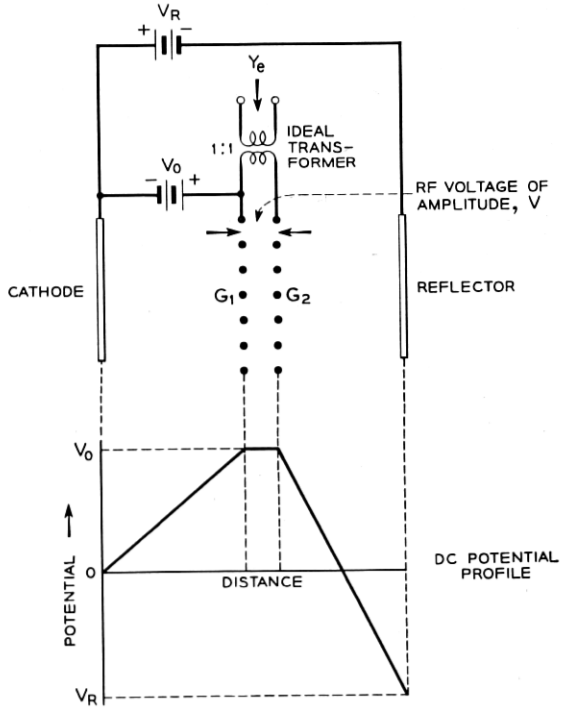

Fig. 1 — Electrode arrangement and dc potential profile giving rise to electronic admittance, Y_e, described by equation (2.1).

with a velocity corresponding to V_0 volts. During their traversal of the interaction gap, i.e., the space bounded by the two grids, this velocity is changed by an amount depending on the instantaneous direction and intensity of the electric field and on the fraction of a cycle spent in traversing the gap. They then enter the retarding dc field of the repeller drift space. Here, they are slowed down, brought to a standstill and returned to the interaction gap for a second transit. During this process, the velocity modulation acquired during the first transit is converted to intensity modulation such that the convection current returning through the gap does so in the form of sharp and well defined pulses with a repetition rate equal to the frequency of the applied RF voltage. This pulsed current may now be harmonically analyzed and its fundamental component evaluated. The ratio of this fundamental component of current to the applied RF voltage is termed electronic admittance, Y_e. Providing the amplitude, V, of the applied RF voltage is small compared to the dc accelerating voltage, V_0, the value of Y_e is given by:

$$Y_e = \frac{I_0 \beta^2 \theta}{2V_0} \frac{2J_1\left(\frac{\beta V \theta}{2V_0}\right)}{\left(\frac{\beta V \theta}{2V_0}\right)} e^{j[(\pi/2)-\theta]}, \tag{2.1}$$

where I_0 = dc beam current.
β = beam coupling coefficient.*
θ = round trip transit time in repeller drift space, in radians.
V_0 = dc beam voltage.
V = amplitude of RF gap voltage.
J_1 = Bessel function operator.

Of all these parameters affecting Y_e we shall focus our attention on two, namely V and θ. The other parameters depend on such factors as tube geometry, electron gun perveance etc. and, within the scope of this investigation, will be considered constant.

Referring to equation (2.1), it is seen that the phase angle associated with Y_e is a function of θ only, whereas the amplitude of Y_e depends on both θ and the RF gap voltage, V. Suppose now θ is held constant while

* β, also referred to as modulation coefficient, is given by

$$\beta = \frac{\sin \frac{\theta_g}{2}}{\frac{\theta_g}{2}}$$

where θ_g, the transit angle in the interaction gap, is expressed in radians.

V is increased from zero to some finite value, a process actually occurring in a reflex klystron during the build-up of oscillations. The amplitude of Y_e will then be of the form $2J_1(x)/x$ and will decrease according to the Bessel function plot of Fig. 2.

For an infinitesimal or zero RF gap voltage the electronic admittance, now referred to as "small-signal" electronic admittance, Y_{es}, may be derived from equation (2.1) as,

$$Y_e|_{V=0} \equiv Y_{es} = \frac{I_0\beta^2}{2V_0}\,\theta e^{j[(\pi/2)-\theta]}. \tag{2.2}$$

When presented in the complex admittance (i.e., g-b) plane, expression (2.2) assumes the form of a geometric spiral as shown in Fig. 4. Each point on the spiral corresponds to a particular value of θ and, since θ is a function of the repeller voltage only, to a particular value of V_R. We also note that for some values of θ the conductance component of Y_{es} is negative while for others it is positive. Thus, there is the possibility of generation of RF energy for values of Y_{es} adjusted by means of the repeller voltage to fall on the left-hand half of the admittance spiral while energy is absorbed for values of Y_{es} having a positive conductance component. As the RF gap voltage, V, builds up from zero to its final value the magnitude of the electronic admittance shrinks along a radius

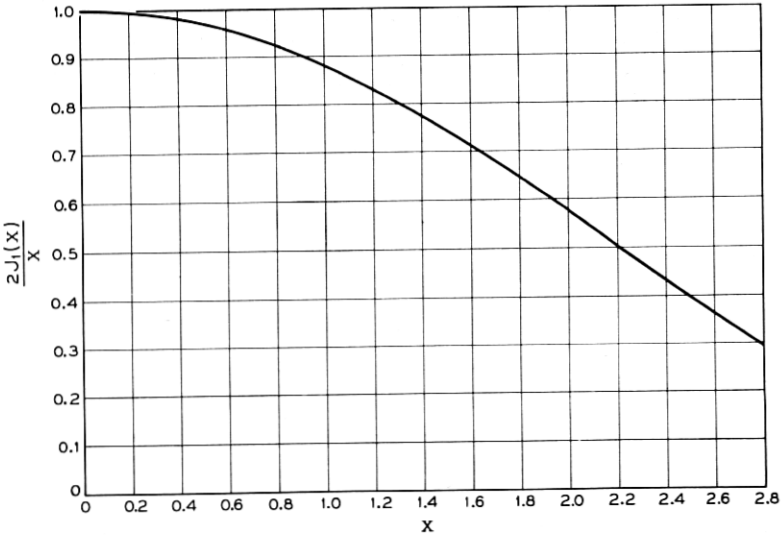

Fig. 2. Bessel function plot showing the relative variation of the amplitude of the electronic admittance (ordinate) as a function of RF gap voltage (abscissa) with repeller drift angle held constant.

vector from Y_{es} to Y_e according to the Bessel function plot of Fig. 2. For $\theta = 2\pi(N + \frac{3}{4})$ radians where $N = 0, 1, 2, 3 \ldots$ the electronic admittance becomes a pure negative conductance as may be seen by putting this relation into equations (2.1) or (2.2).

Summarizing, we have seen that the presence of an electron stream bunched in accordance with the arrangement of Fig. 1 gives rise to an admittance appearing across the grids bounding the interaction space. The phase angle of this admittance is a function only of the repeller drift angle, θ, while its magnitude depends on both θ and the RF gap voltage, V. For values of θ in the vicinity of $2\pi(N + \frac{3}{4})$ radians the conductance component is negative, a necessary condition for the production of sustained oscillations.

2.2 *Passive Circuit Admittance of Single Resonator*

Any resonant cavity may be represented by a simple parallel *G-C-L*-combination provided the desired resonance is sufficiently far removed from adjacent ones. In some cases such as in cylindrical or waveguide cavities, to name two, it is difficult to ascribe physical significance to the lumped elements appearing in the equivalent circuit representation. This is not so in the case of a conventional reflex klystron cavity. Since the latter always consists of a re-entrant type resonator, most of the electric field is concentrated in the interaction gap, i.e., the narrow region traversed by the outgoing and returning electrons and bounded by two parallel grids, while the major portion of the magnetic flux resides in the outer cylindrical section. Thus, the effective shunt capacitance appearing in the equivalent circuit is associated primarily with the above grid planes, a minor contribution originating in the fringing field close to the re-entrant post and the residual electric field in the outer cylindrical part of the cavity.

The input admittance, Y, of a high Q resonator when represented by C, L, and G connected in parallel is given by,

$$Y = G(1 + j2Q\delta) \tag{2.3}$$

$$= G + j2C\Delta\omega, \tag{2.4}$$

where $Q = \omega_0 C/G$ and $\delta = \Delta\omega/\omega_0 = \Delta f/f_0 = (f - f_0)/f_0$, and G represents all internal resonator losses plus the external load referred to the gap. Plotted in the complex admittance plane, the locus of the admittance vector with varying frequency is a straight line parallel to the imaginary axis and spaced a distance corresponding to G to its right. The variation in susceptance is directly proportional to the frequency deviation

from resonance. Also, the frequency deviation required to bring about a given change in susceptance is inversely proportional to both C and Q.

2.3 *Equivalent Circuit of Single Resonator Reflex Klystron*

We saw that the presence of a bunched electron stream between two closely spaced grid planes gives rise to an electronic admittance the properties of which were discussed earlier. Suppose we now let these grids become part of a re-entrant cavity so that they form the boundaries of the interaction space. This will make them elements of significance and common to both the electron stream and the passive circuit admittance. As far as the electron stream is concerned the grids become the terminals across which the electronic admittance, Y_e, is developed and in relation to the resonant circuit they constitute the major portion of the effective

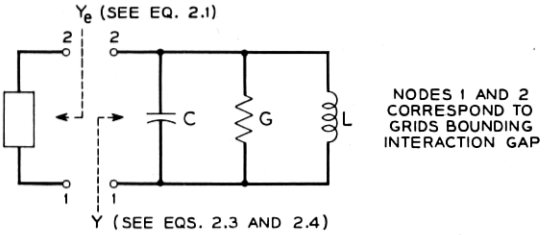

Fig. 3. — Equivalent circuit of single resonator reflex klystron.

shunt capacitance. Based on these remarks, it should be apparent that a single-resonator reflex klystron may be represented by an equivalent circuit consisting of a parallel combination of Y_e, C, G, and L as shown in Fig. 3. Furthermore, the expressions for Y_e and Y as given by equations 2.1 and 2.4, respectively, show that these two quantities are independent of each other. The electronic admittance, Y_e, is a function of the electron optics of the tube, while the passive circuit admittance, Y, is a function purely of cavity parameters, including the tightness of coupling to the external load.

2.4 *Performance Analysis Based on Complex Admittance Plane Representation*

The condition for oscillation applying to the equivalent reflex klystron circuit requires the total admittance across nodes 1 and 2 of Fig. 3 to equal zero, i.e.,

$$Y_e + Y = 0, \qquad 2.5a$$

or

$$Y_e = -Y. \qquad 2.5b$$

Attainment of this condition is preceded by a period during which the RF gap voltage increases from its initial, near-zero value to its final steady state amplitude. Concurrently, the net conductance across nodes 1 and 2 changes from its maximum negative value to zero and the electronic admittance vector shrinks from Y_{es} to Y_e.

This process of build-up of oscillations and the final steady state may be conveniently studied by the graphical representation of Fig. 4. Here, the negative of the passive circuit admittance, Y, has been superimposed on the small-signal electronic-admittance spiral. Since the net conductance across the interaction gap (nodes 1 and 2 in Fig. 3) must be negative in order for oscillations to build up, we see at once that the $(-Y)$ plot, sometimes also referred to as "load line," divides the complex admittance plane into two regions: the one to its left, in which the

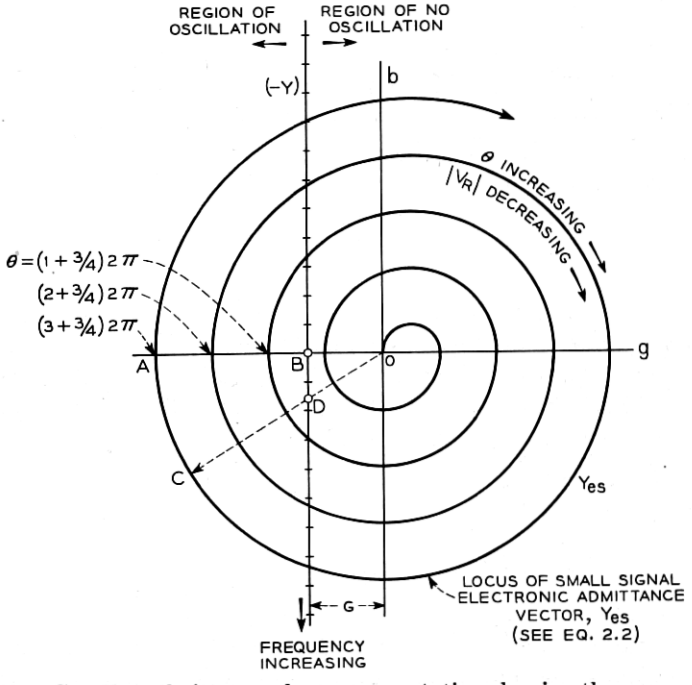

Fig. 4 — Complex admittance plane representation showing the superposition of the negative of the circuit input admittance upon the small signal electronic admittance spiral. Each point on spiral corresponds to a particular value of repeller transit angle, θ, and hence repeller voltage, V_R, and each division on the $(-Y)$ locus to an equal frequency increment.

negative electronic conductance exceeds the circuit conductance and where the build-up of oscillations is possible, and the region to its right where the condition for the build-up of oscillations is not met. Thus, for the load line in the position indicated, the tube will not oscillate in the $N = 0$ mode, but will do so in the $N = 1, 2, 3$ and higher order modes.

Still referring to Fig. 4, suppose θ has been adjusted by means of the repeller voltage to $\theta_1 = (3 + \frac{3}{4})2\pi$ radians, i.e., the center of the $3 + \frac{3}{4}$ mode. The small signal-electronic-admittance vector will then be a pure negative conductance terminating on the spiral at point A and together with the passive circuit conductance yielding a net negative conductance across the grids of value $(\overline{OA}\text{-}\overline{OB})$. Oscillations, therefore, will build up until the equilibrium condition, $Y_e = -Y$, has been satisfied. In terms of the admittance plane representation, the electronic-admittance vector will shrink without change in its phase until it terminates on the load line at point B. Since the electronic admittance for the particular value of θ chosen is a pure conductance, oscillations will occur at the resonant frequency of the cavity, f_0, which is also the frequency corresponding to the intersection of the electronic-admittance vector and the load line.

From equation 2.1 we see that,

$$\frac{\overline{OB}}{\overline{OA}} = \frac{\dfrac{2J_1\left(\dfrac{\beta V_1\theta_1}{2V_0}\right)}{\left(\dfrac{\beta V_1\theta_1}{2V_0}\right)}}{\left[\dfrac{2J_1\left(\dfrac{\beta V\theta}{2V_0}\right)}{\left(\dfrac{\beta V\theta}{2V_0}\right)}\right]_{V=0}} = \frac{2J_1\left(\dfrac{\beta V_1\theta_1}{2V_0}\right)}{\left(\dfrac{\beta V_1\theta_1}{2V_0}\right)}, \tag{2.6a}$$

where V_1 is the steady state RF gap voltage corresponding to drift angle, θ_1. Entering the graph of Fig. 2 with $\overline{OB}/\overline{OA}$ as the ordinate, we can read off the corresponding value of $(\beta/2V_0)V_1\theta_1$. For a particular tube structure and operating conditions, $\beta/2V_0$ will be a fixed constant so that, in effect, we have determined the value of a quantity proportional to the product of $V_1\theta_1$.

Next, consider the case where θ has been changed from $\theta_1 = (3 + \frac{3}{4})2\pi$ to $\theta_2 = K(3 + \frac{3}{4})2\pi$ radians. The electronic admittance vector for $V = O$ will now terminate on the Y_{es}-plot at C. Again a build-up of oscillations will ensue and upon attainment of the steady state condition the vector will have shrunk to the value $\overline{OD}$, with the

frequency of oscillation determined by the location of point D on the load line. By an argument similar to the one used before, we have

$$\frac{\overline{OD}}{\overline{OC}} = \frac{2J_1\left(\frac{\beta V_2\theta_2}{2V_0}\right)}{\left(\frac{\beta V_2\theta_2}{2V_0}\right)} \tag{2.6b}$$

and once more, the plot of Fig. 2 will yield the value of

$$\left(\frac{\beta}{2V_0}\right)V_2\theta_2 \qquad \text{or} \qquad \left(\frac{\beta}{2V_0}\right)KV_2\theta_1 .$$

It is apparent that $\beta/2V_0$ is a factor common to all these determinations and may be neglected if we are only interested in the mode shape, i.e. the *relative* variation of gap voltage or output power with the repeller drift angle, θ. For modes higher than $N = 2$, the electronic admittance spiral approximates a number of semi-circles with their centers close to the origin. Hence

$$\overline{OA} \approx \overline{OC} \qquad \text{and} \qquad \frac{\overline{OD}}{\overline{OC}} > \frac{\overline{OB}}{\overline{OA}} .$$

Figure 2, then indicates that

$$V_1\theta_1 > V_2\theta_2 \qquad \text{or} \qquad V_1\theta_1 > KV_2\theta_1$$

and since K does not vary greatly from unity $V_1 > V_2$. This is as it should be since we know that a change in repeller voltage from its mid-mode value causes a decrease in power output and, hence, in gap voltage. The latter will decrease to zero when θ has been adjusted to a value such that the Y_{es} vector terminates at the intersections of the electronic admittance spiral and the load line.

Another result which becomes apparent from an inspection of Fig. 4 is this. For the condition of stable oscillation the phase angle of the electronic admittance equals that of the passive circuit except for an additive constant of 180 degrees which, however, may be disregarded in this argument. The frequency of oscillation may be determined from the input-phase-angle vs. frequency plot of the passive circuit by looking up the frequency corresponding to the particular value of phase angle to which the electronic admittance has been adjusted (by means of repeller voltage). Thus, the curve relating repeller-drift-angle to frequency is identical with the plot of input-phase-angle vs. frequency for the passive circuit. Moreover, if repeller voltage is linearly related

to the repeller-drift-angle, a condition which in most practical cases holds over a restricted repeller voltage swing about its midmode value, then the repeller voltage-frequency plot will have the same shape as the input phase angle-frequency curve of the passive circuit, differing from the latter only by a constant multiplying factor. We therefore conclude that the modulation performance of the reflex klystron, at least over the central portion of the mode, may be predicted from an examination of the driving point properties of the passive circuit.

The above method of graphical analysis is quite useful in the case of conventional reflex klystrons, although the same results may be obtained analytically by making use of the equation for electronic admittance in conjunction with that of the input admittance of a single resonator. In the case of coupled resonators the expression for input admittance becomes much more involved, as we shall see later, with the result that the graphical approach outlined above was found by far the quicker and more practical method of solution.

3.0 THEORY OF COUPLED RESONATOR REFLEX KLYSTRON

It has been shown that the performance of a reflex klystron can be analyzed by considering the electronic and passive circuit admittances separately and then combining the two graphically in the complex admittance plane. The same procedure can be adopted in the determination of mode shapes resulting from the interaction of the electronic admittance with any arbitrary circuit admittance which can be realized across the gap. Conversely, we can determine the admittance or impedance function required to produce a particular desired mode shape. In other words: given an admittance function, we can determine the resulting mode shape, and given a desired mode shape, we can predict the required admittance function. As an example, consider a mode having a flat top and vertical sides as shown in Fig. 5(a). This would be the ideal shape for a reflex oscillator to be used as an electronically swept signal source. To achieve this mode shape, we must realize an admittance function across the bunching grids yielding a constant excess of negative electronic admittance over a range of repeller voltages. Such a function is shown in the complex admittance plane along with the plot of Y_{es} in Fig. 5(b) and the corresponding input impedance in 5(c). It will result in a frequency range of constant RF gap voltage which in turn will give rise to a range of flat power provided it is developed across a constant, frequency-invariant conductance. In order to clarify this rather important consideration, let us write the admittance appearing

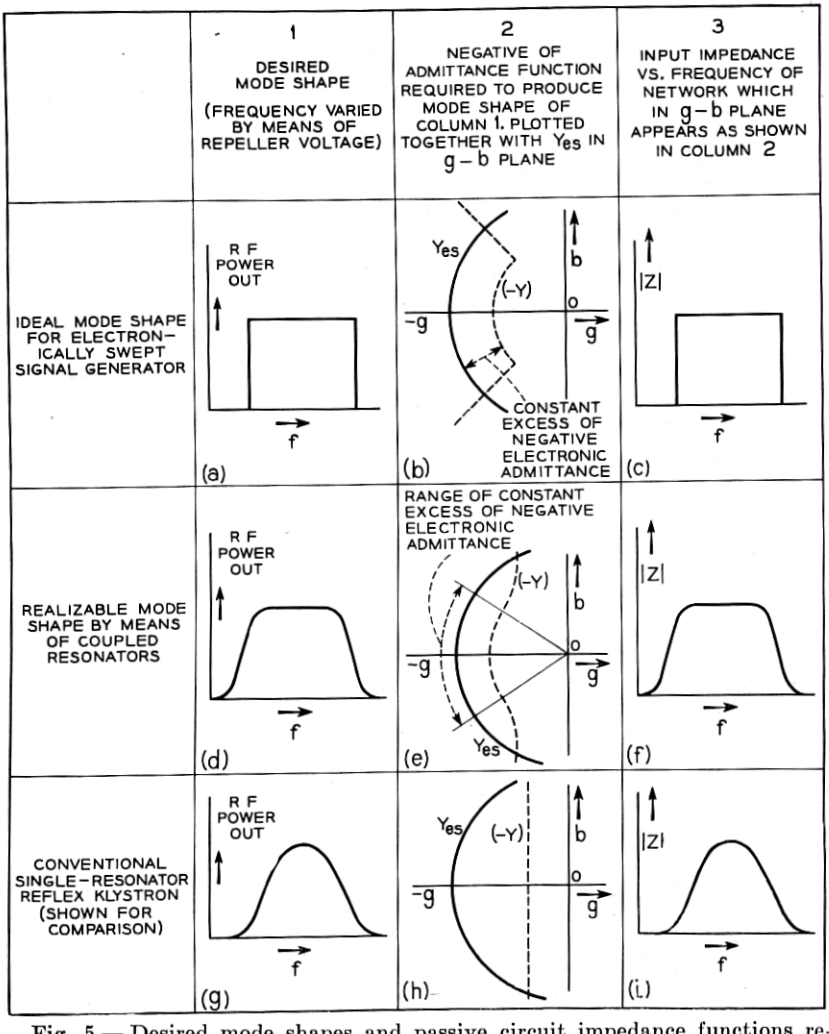

Fig. 5 — Desired mode shapes and passive circuit impedance functions required to produce them.

across the interaction gap as,

$$Y = G_T(f) + jB_T(f),$$

where $G_T(f)$ and $B_T(f)$ denote the total conductance and total susceptance both of which are functions of frequency. Over the region of constant RF gap voltage we require $| Y |$ or

$$\sqrt{G_T^2(f) + B_T^2(f)}$$

to be constant. This, however, means that the power generated (as distinct from the power delivered to the load) is not constant since it is given by,

$$\text{Generated Power} = \tfrac{1}{2}(\text{RF gap voltage})^2 \text{ (Total Conductance)}$$
$$= \tfrac{1}{2}V^2G_T(f)$$

and G_T varies with frequency. Now, the term $G_T(f)$ is the sum of a number of conductances, all but one of which do not change with frequency. The frequency-invariant conductances represent the different power losses in the primary resonator plus the external load referred to the gap while the remaining frequency-sensitive conductance is due to the coupled circuit used in shaping the admittance locus. Hence the useful power output is proportional to V^2 and therefore constant if V^2 is constant, whereas the variation with frequency of the total conductance must be taken into account in evaluating generated power.

The foregoing discussion together with the illustrations of Fig. 5 should make it clear that in order to maintain a constant RF power output level, over a specified frequency range, we must have the electronic admittance interact with a circuit the input impedance of which, when referred to the gap, is also constant over the same frequency range. A circuit having such characteristics can be obtained by the use of coupled resonators as will be shown later.

Suppose the emphasis is on modulation linearity rather than flatness of power output. Attention, then, must be focused on the relation between input phase angle and frequency of the passive circuit. Here, again, we shall see that the application of coupled resonators offers advantages beyond what is possible with a single cavity.

3.1 *Driving Point Properties of Two Coupled Resonators Having Equal Q's*

Using the equivalent shunt representation as shown in Fig. 6, the exact expression for the input admittance, Y, of two coupled resonators

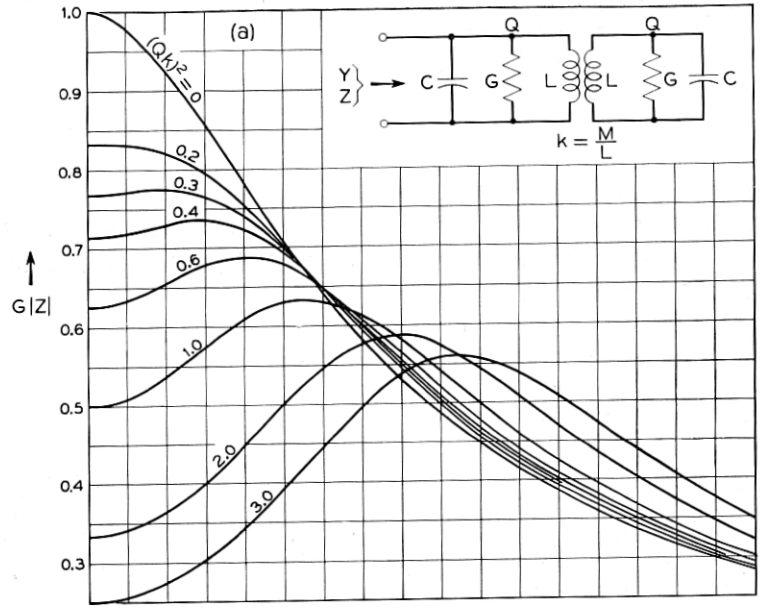
(a)
Q
Q
Y
Z
C
G
L
L
G
C
k = M/L
G|Z|
(Qk)² = 0
0.2
0.3
0.4
0.6
1.0
2.0
3.0
1.0
0.9
0.8
0.7
0.6
0.5
0.4
0.3

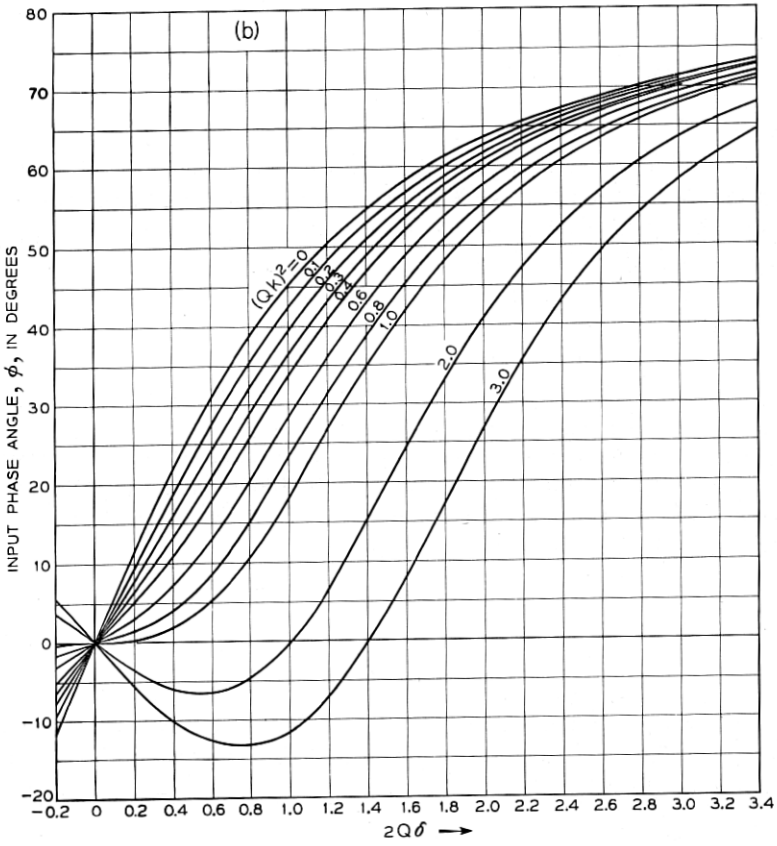
(b)
INPUT PHASE ANGLE, φ, IN DEGREES
(Qk)² = 0
0.1
0.2
0.3
0.4
0.6
0.8
1.0
2.0
3.0
80
70
60
50
40
30
20
10
0
−10
−20
−0.2
0
0.2
0.4
0.6
0.8
1.0
1.2
1.4
1.6
1.8
2.0
2.2
2.4
2.6
2.8
3.0
3.2
3.4
2Qδ

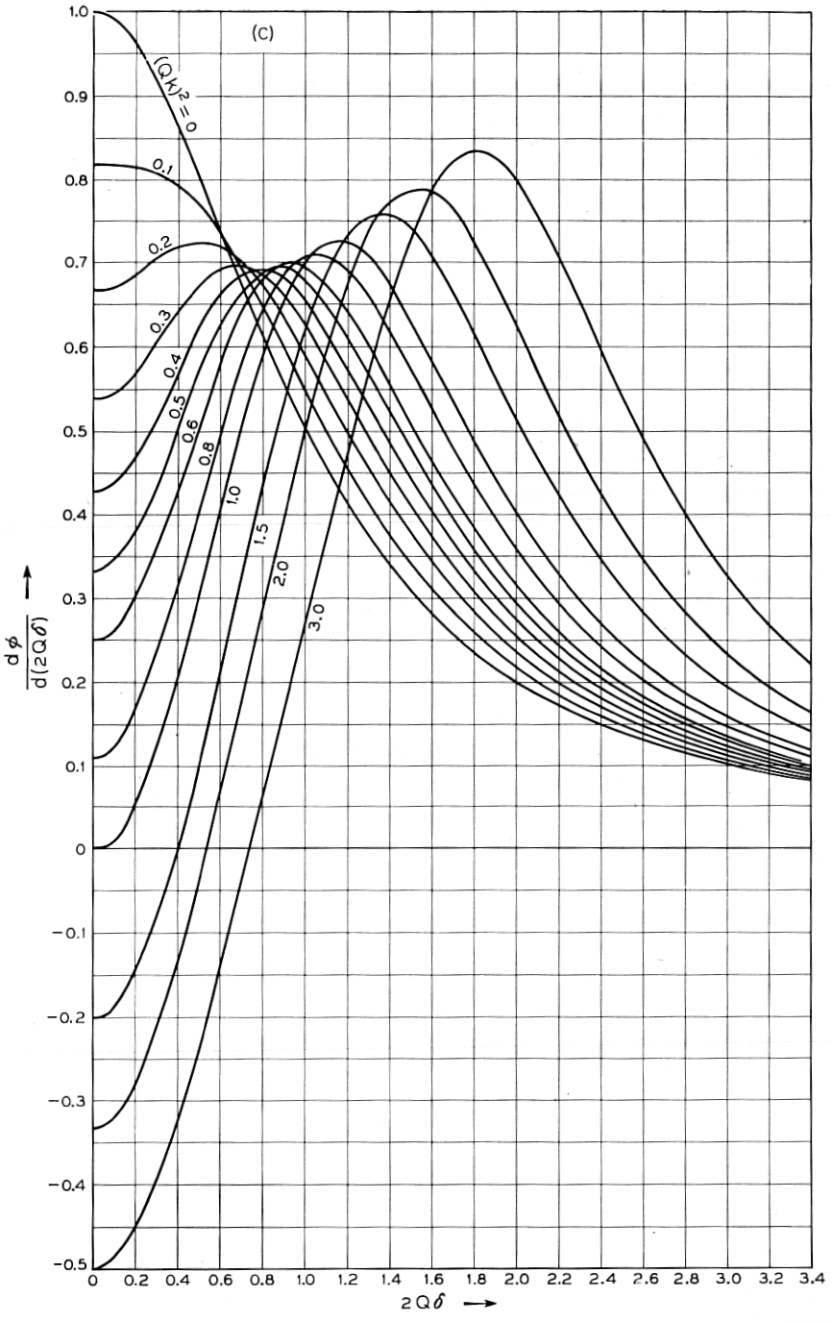

Fig. 6 — Normalized driving point properties of two coupled, synchronously tuned resonators having equal Q's. (a) Input impedance, $G|\bar{Z}|$, versus frequency deviation from resonance, $2Q\delta$, for various degrees of coupling, Qk. (b) Input phase angle, ϕ, versus frequency deviation. (c) Rate of change of ϕ with $2Q\delta$ versus $2Q\delta$.

having equal Q's and equal resonant frequencies is given by,

$$Y = G(g + jb),$$

where

$$b = \frac{Q(\Omega^2 m - 1)}{\Omega m}\left(1 - \frac{\left(\frac{Qk}{\Omega m}\right)^2}{1 + \left[\frac{Q(\Omega^2 m - 1)}{\Omega m}\right]^2}\right),$$

$$g = 1 + \frac{\left(\frac{Qk}{\Omega m}\right)^2}{1 + \left[\frac{Q(\Omega^2 m - 1)}{\Omega m}\right]^2}. \tag{3.1}$$

G = shunt conductance of primary and secondary resonators.

g, b = total input conductance and susceptance respectively normalized with respect to G,

Ω = normalized frequency $= f/f_0$.

f_0 = resonant frequency of both primary and secondary resonators.

k = coefficient of coupling.

$m = 1 - k^2$.

This expression for input admittance, though accurate, is rather unwieldy because of the many variables involved. A few obvious approximations, however, will change equation (3.1) into a much simpler and more meaningful expression, yet sufficiently accurate for the range of Q's and bandwidths of interest here. Let,

$$\Omega = \frac{f}{f_0} = \frac{f_0 + \Delta f}{f_0} = 1 + \frac{\Delta f}{f_0} = 1 + \delta,$$

where δ denotes the normalized frequency deviation from resonance, $\Delta f/f_0$. If we further assume that $k^2 \ll 1$ and the range of Q's is such that $(Qk)^2$ may vary from zero to about five and that the maximum value of δ is small enough so that its higher powers may be neglected, then equation (3.1) may be simplified to,

$$\frac{Y}{G} = \left[1 + \frac{(Qk)^2}{1 + (2Q\delta)^2}\right] + j2Q\delta\left[1 - \frac{(Qk)^2}{1 + (2Q\delta)^2}\right]. \tag{3.2}$$

The above equation* essentially contains three variables:

(a) The dependent variable, Y/G, i.e. input admittance normalized with respect to the shunt conductance,

(b) the independent variable, $(2Q\delta)$, which is a factor proportional to the frequency deviation from resonance, and

(c) parameter, (Qk), a measure of the tightness of coupling between the two cavities.

Compared with the input admittance for a single resonator which was given earlier, [equation (2.3),] as, $Y/G = 1 + j2Q\delta$, it is seen that the conductance component has been changed by a factor

$$\left[1 + \frac{(Qk)^2}{1 + (2Q\delta)^2}\right]$$

and the susceptance by

$$\left[1 - \frac{(Qk)^2}{1 + (2Q\delta)^2}\right].$$

Also, by setting $k = 0$, i.e., completely decoupling the secondary resonator, equation (3.2) reduces to equation (2.3) as, indeed, it should.

The information contained in equation (3.2) may be presented graphically in a number of ways. We can plot the magnitude of the normalized input impedance, $G|\ Z\ |$, as a function of $2Q\delta$ with $(Qk)^2$ as parameter as shown in Fig. 6(a).† Or we can plot the input admittance given by equation (3.2) directly in the g-b plane as in Fig. 7. Finally, we may show the variation of input phase angle with normalized frequency for different degrees of coupling as in Fig. 6(b). Each of these graphical representations has an important bearing on the performance of the coupled resonator klystron. Thus, the curves of Fig. 6(a) will have the same general shape as the RF power output vs. frequency plot of the reflex oscillator, the family of curves of Fig. 7, when superimposed on the electronic admittance spiral, can be used for a detailed analysis of mode shapes, and Fig. 6(b) determines the modulation characteristics obtainable with coupled resonators.

Having briefly touched upon the significance of the families of curves given in Figs. 6(a), 7, and 6(b), we can now proceed to discuss them in greater detail and to establish further valuable results.

* To check the accuracy of this equation, the curve for $(Qk)^2 = 1$ in Fig. 6(a) was replotted using the full expression given by equation 3.1 and assuming $Q = 100$. The agreement was found to be essentially perfect as far as its use in this investigation is concerned.

† For a similar presentation of the *transfer* characteristics of coupled tuned circuits see reference (6).

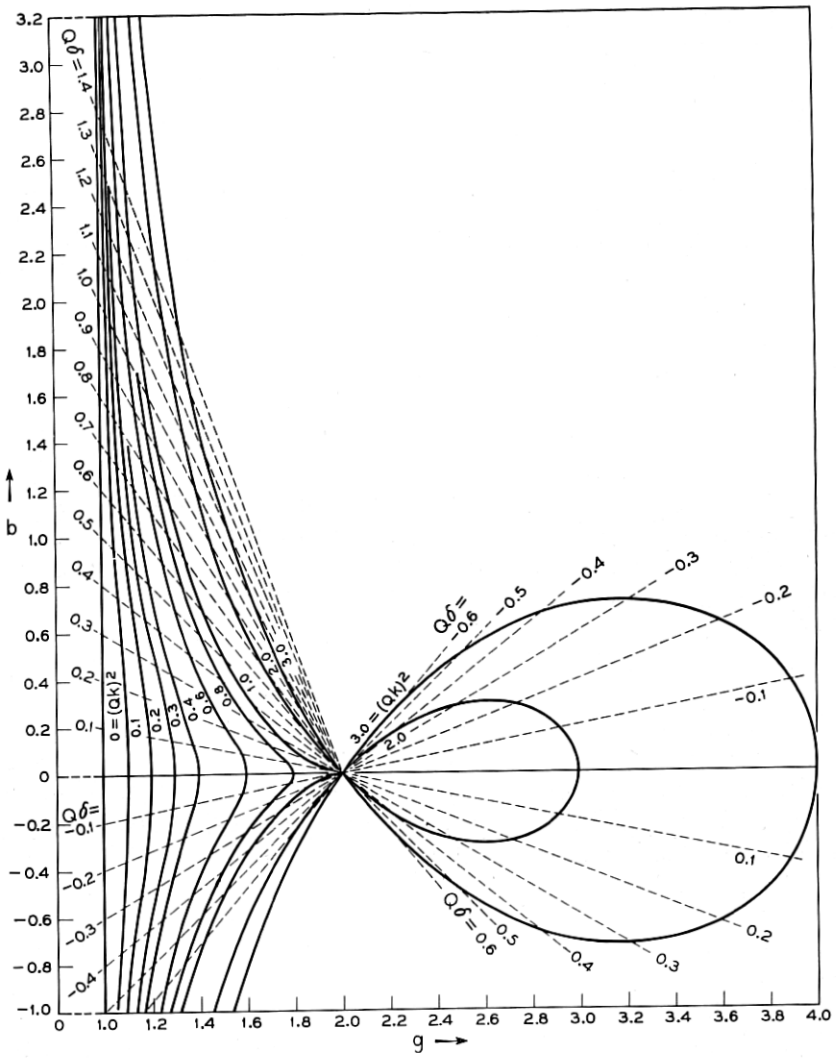

Fig. 7 — Input admittance of circuit shown in Fig. 6 plotted in g–b plane. Solid lines are loci of input admittance vectors, dashed lines connect points of equal frequencies.

3.1.1 *Variation of Input Impedance with Frequency, Fig. 6(a).* Equation 3.2 may be written as

$$\frac{Y}{G} = g + jb, \tag{3.3}$$

where

$$g = \left[1 + \frac{(Qk)^2}{1 + (2Q\delta)^2}\right] \tag{3.4}$$

and

$$b = 2Q\delta\left[1 - \frac{(Qk)^2}{1 + (2Q\delta)^2}\right]. \tag{3.5}$$

Hence

$$\frac{|Y|}{G} = \sqrt{g^2 + b^2}$$

and

$$G|Z| = \frac{1}{\sqrt{g^2 + b^2}}. \tag{3.6}$$

It is seen that g^2 and b^2 involve even powers of $(2Q\delta)$ only, so that $G|Z|$ is an even function, i.e., symmetrical about the vertical axis. For this reason, one-half the normalized impedance plot only has been given in Fig. 6(a). Inspection of this figure reveals that the effect of coupling to a secondary resonator is to broaden the frequency range over which a high impedance level can be maintained across the interaction gap. Comparing the variation of input impedance with frequency for $(Qk)^2 = 0$ (i.e., single cavity) with that for $(Qk)^2 = 0.3$, we see that for a frequency deviation of $2Q\delta = \pm 0.6$ the former shows a drop of 14 per cent while the latter only varies by ± 0.58 per cent. In terms of two coupled resonators having $Q = 100$ and operating at 4000 mc this means a variation in impedance of only ± 0.58 per cent or $\pm .052$ db over a frequency range of 24 mc.

Another result clearly brought out by the family of curves of Fig. 6(a) is that the process of broadbanding by coupling to a second resonator results in a reduction in absolute impedance level. This reduction in impedance level at midband is related to the tightness of coupling, $(Qk)^2$, by the expression,

$$[G|Z|]_{\delta=0} = \frac{1}{1 + (Qk)^2}, \tag{3.7}$$

which may be readily derived from eq. 3.6. Note that for $(Qk)^2 = 1$, the impedance level at midband has dropped to half the value obtained with a single resonator or $(Qk)^2 = 0$. The degree of coupling corresponding to $(Qk)^2 = 1$ is noteworthy for reasons other than the one just mentioned. They will be discussed in the following section.

3.1.2 *Input Admittance Plot in g-b Plane, Fig. 7.* The graphical representation of input admittance in the complex admittance plane is of particular usefulness in the analysis of the coupled resonator reflex klystron. For the moment, however, we shall restrict the discussion to a consideration of the passive circuit only.

Each solid line in Fig. 7 is the locus of the admittance vector for a particular tightness of coupling. For $(Qk)^2 = 0$ the locus is a straight line parallel to the susceptance axis as described earlier for the case of a single resonator. For $(Qk)^2 = 0.3$ the shape of the locus approximates a circle with its center at the origin; this, of course, being true only over a restricted frequency range. As the coupling to the secondary resonator is progressively tightened, the locus is seen to bulge out in the direction of increasing conductance until, for $(Qk)^2 = 1$, it forms a cusp. This condition will henceforth be referred to as "critical coupling."* Coupling even tighter causes the formation of loops of increasing size.

For the overcoupled case, $(Qk)^2 > 1$, the admittance-vector locus crosses the conductance axis three times, with the first and third crossings coincident and independent of $(Qk)^2$ and the second crossover a function of $(Qk)^2$. The location of these intersections with the g-axis may be determined by equating the susceptance to zero, i.e., from equation (3.5),

$$2Q\delta \left[1 - \frac{(Qk)^2}{1 + (2Q\delta)^2} \right] = 0.$$

Hence the crossing to the extreme right occurs for $2Q\delta = 0$ while the first and third interesections correspond to

$$2Q\delta = \pm\sqrt{(Qk)^2 - 1}.$$

To determine the size of the loop we substitute $2Q\delta = 0$ into the expression for the conductance, i.e., equation (3.4) and obtain,

$$g|_{2Q\delta=0} = 1 + (Qk)^2,$$

* It should be noted that the term "critical coupling" as applied to the *transfer* characteristics of coupled tuned circuits, though also occuring for $(Qk)^2 = 1$, assumes a different significance in that it describes the condition of maximum flatness in response and optimum phase linearity. (See reference 6.) In the case of the coupled resonator reflex klystron, "critical coupling" forms the transition between stable performance and load hysteresis as will be shown later.

showing that the size of the loop is a sensitive function of the degree of coupling. The conductance value for the first and third crossover points is obtained by substituting

$$2Q\delta = \pm\sqrt{(Qk)^2 - 1}$$

into equation (3.4) and results in $g = 2$, i.e., a value of g independent of the coupling coefficient.

The dashed lines shown in Fig. 7 connect points of equal frequencies. It is of interest to note that these loci are straight lines crossing the conductance axis at $g = 2$. To prove this, eliminate $(Qk)^2$ between equations (3.4) and (3.5). This yields,

$$g - 1 = 1 - \frac{b}{2Q\delta},$$

whence

$$b = (-2Q\delta)(g - 2). \tag{3.8}$$

For a particular and constant value of $2Q\delta$, equation (3.8) describes a straight line of slope equal to $(-2Q\delta)$ intersecting the g-axis at $g = 2$.

3.1.3 *Variation of Input Phase Angle with Frequency, Fig. 6(b).* The last driving point property of interest to this study is the dependence upon frequency of the input phase angle, ϕ. Referring to equation (3.2), this quantity is obtained as,

$$\phi = \tan^{-1}\left[2Q\delta\,\frac{1 + (2Q\delta)^2 - (Qk)^2}{1 + (2Q\delta)^2 + (Qk)^2}\right]. \tag{3.9}$$

The graphical representation of this function is given in Fig. 6(b). It shows the gradual transition from a simple S-shaped curve for $(Qk)^2 = 0$, having its only point of inflection at the origin, to the type of curve corresponding to $(Qk)^2 > 1$ which intersects the frequency axis three times. The special case of $(Qk)^2 = 1$, considered earlier and found to result in the formation of a cusp in the complex admittance plane, now gives rise to a plot of input phase which is tangent to the horizontal axis at the origin.

To investigate the condition for greatest linearity between phase angle and frequency, which, when applied to the coupled resonator reflex klystron, would be the condition for optimum modulation linearity, one could simply apply a straight edge to the curves of Fig. 6(b) and pick the best value of $(Qk)^2$ in this manner. A much more sensitive criterion of linearity, however, is the variation with frequency of the slope of these curves. An analytical expression for this slope has been

derived from equation (3.9) as,

$$\frac{d\phi}{d(2Q\delta)} = \frac{[1 - (Qk)^4] + (2Q\delta)^2[2 + 4(Qk)^2] + (2Q\delta)^4}{[1 + (Qk)^2]^2 + (2Q\delta)^2[3 + (Qk)^4] + (2Q\delta)^4[3 - 2(Qk)^2] + (2Q\delta)^6}. \tag{3.10}$$

The above expression, involving even powers of $2Q\delta$ only, results in a family of curves symmetrical about the vertical axis, the positive half of which is shown in Fig. 6(c). From it the value of $(Qk)^2$ for greatest linearity or most constant slope is seen to lie somewhere between 0.1 and 0.2. This is further borne out by Fig. 8, in which this region has been more fully explored. Fig. 8 constitutes a plot quite similar to that

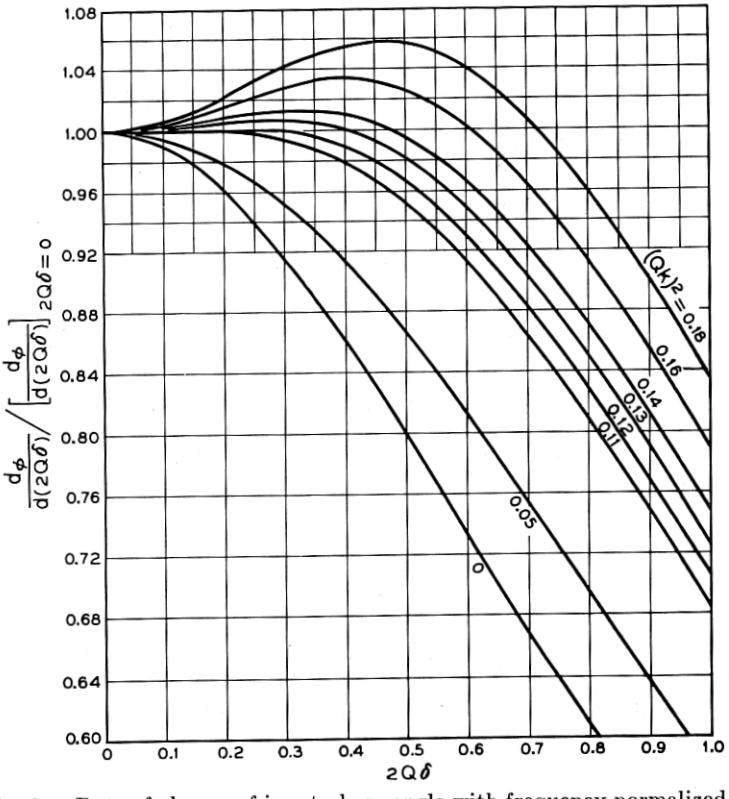

Fig. 8 — Rate of change of input phase angle with frequency normalized with respect to its center value for the circuit shown in Fig. 6. This quantity, the constancy of which is a measure of phase angle versus frequency linearity, is seen to stay absolutely constant over a frequency range corresponding to $2Q\delta = \pm 0.3$ for $(Qk)^2 = 0.12$ while the single resonator case, i.e. $(Qk)^2 = 0$, shows a change of 8% over the same frequency range.

of Fig. 6(c) except that the ordinate now represents the instantaneous slope normalized with respect to its midmode value. The curves shown are for values of $(Qk)^2$ ranging from zero to $(Qk)^2 = 0.18$. Let us, for example, examine the curve corresponding to $(Qk)^2 = 0.12$; the slope is seen to stay absolutely constant up to a frequency deviation of $2Q\delta = \pm 0.3$, while the plot for the single resonator, i.e., $(Qk)^2 = 0$, included in this figure for comparison, changes by 8.4 per cent over the same frequency range.

Putting this in another way, suppose the maximum allowable deviation in slope from its mid-band value is one per cent. Fig. 8 then indicates that the permissible frequency deviation for coupled resonators having a value of $(Qk)^2 = 0.135$ is given by $2Q\delta = \pm 0.5$, whereas it must be restricted to one-fifth this value, i.e., $2Q\delta = \pm 0.1$, for the single resonator case. In terms of a midband frequency of 4000 mc and $Q = 100$, the permissible frequency excursions would be ± 10 mc and ± 2mc, respectively.

It is to be noted that the value of coupling coefficient resulting in greatest modulation linearity is considerably smaller than the value of coupling coefficient found to yield a constant impedance level.

3.2 *Mode Shapes Resulting from the Interaction Between Electronic Admittance and Input Admittance of Two Coupled Resonators of Equal Q's*

Having determined all relevant properties of the passive circuit as they appear across the grids of the bunching gap, we may now proceed to investigate the results arising from their interaction with the electronic admittance. The approach to be adopted is essentially the same as the one outlined earlier for the case of the conventional single-cavity reflex klystron. It involves a graphical superposition of the negative of the passive circuit admittance upon the small-signal-electronic-admittance spiral in the g-b plane, such as shown in Fig. 9(a). The location of the load lines with respect to the spiral has been chosen, somewhat arbitrarily, such that the ratio between the length of the Y_{es}-vector corresponding to $\theta = (2 + \frac{3}{4})$ cycles and that of the input admittance vector for $(Qk)^2 = 0$ and $\delta = 0$ equals two. Load lines have been drawn for five values of $(Qk)^2$ ranging from zero to unity.

The determination of mode shapes from Fig. 9(a) proceeds as illustrated in Table I. Taking the repeller drift angle as the independent variable we can obtain corresponding values of generated power (in arbitrary units) and frequency (in terms of $Q\delta$) by going through the steps indicated.

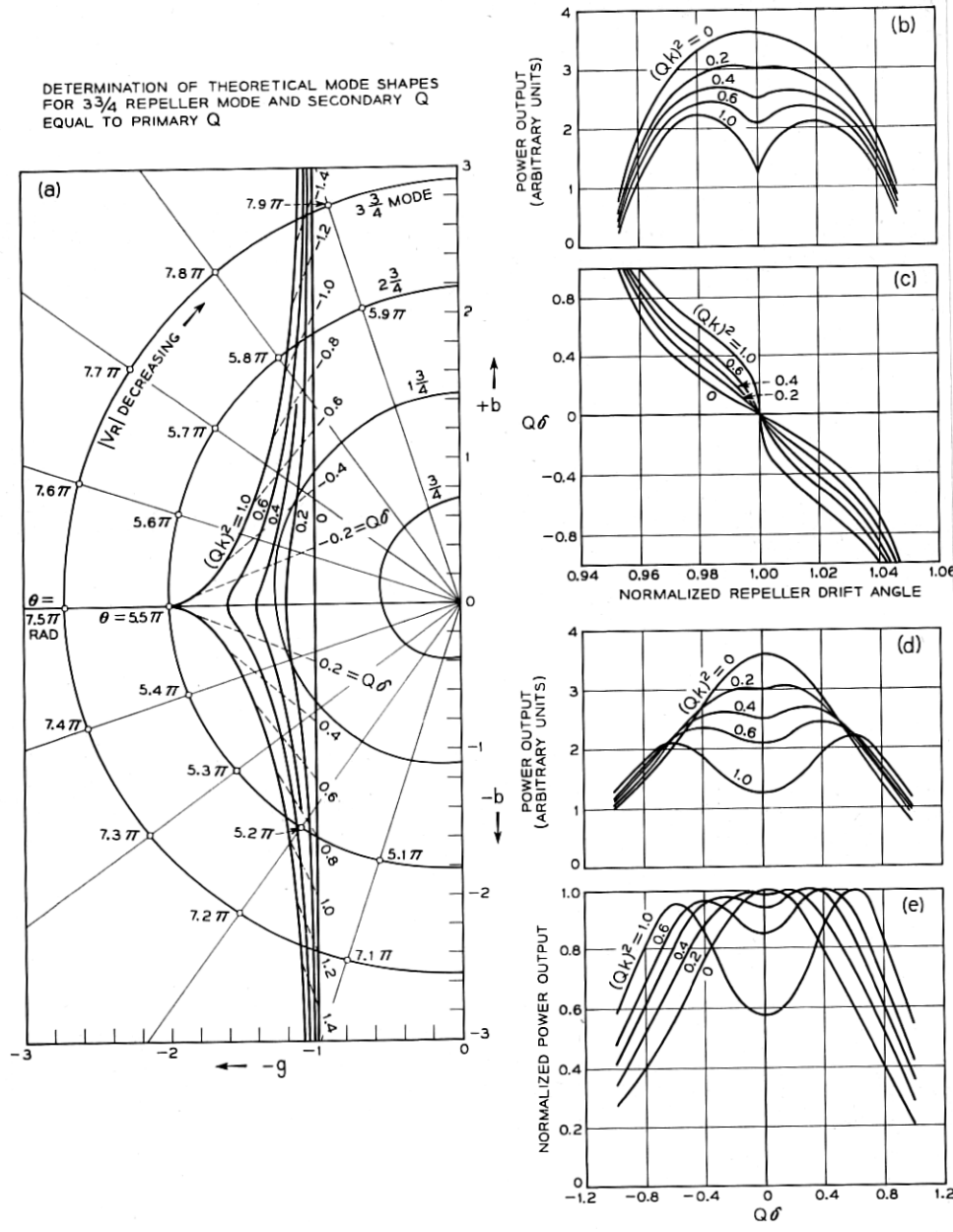

Fig. 9 — Graphical determination of mode shapes for a coupled resonator reflex klystron having the secondary cavity Q equal to primary Q. (a) Load lines for various degrees of coupling superimposed on small signal electronic admittance spiral. (b) Power output versus repeller drift angle. (c) Frequency versus repeller drift angle. (d) Power output versus frequency. (e) Power output, normalized with respect to its maximum value within the mode, shown as a function of frequency.

TABLE I — DETERMINATION OF MODE SHAPES FROM COMPLEX ADMITTANCE PLANE PLOT OF FIGURE 9(a)

(1)	(2)	(3)	(4)	(5)	(6)	(7)	(8)	(9)
$K\theta_0$, Repeller Drift Angle (θ_0 = Midmode Value)	K, Ratio of Drift Angle to its Midmode Value	Small Signal Electronic Admittance	Passive Circuit Admittance	$\frac{2J_1(KV\theta_0)}{(KV\theta_0)}$ i.e. (4)/(3)	$(KV\theta_0)$ from Bessel-function plot of Fig. 2	$V\theta_0$, (6)/(2)	$(V\theta_0)^2$, Quantity Proportional to Power Output	$Q\delta$
		Measured off Fig. 9(a) in Arbitary Units of Length						
$(Qk)^2 = 0.4$, $2\frac{3}{4}$-mode, i.e., $\theta_0 = (2 + \frac{3}{4})2\pi$ radians $= 5.5\pi$ radians								
5.20π	0.947	9.45	9.45	1.000	0.00	0.000	0.00	+0.85
5.25π	0.955	9.54	8.10	0.849	1.13	1.182	1.40	+0.67
5.30π	0.967	9.63	7.35	0.764	1.44	1.493	2.23	+0.53
5.35π	0.974	9.72	6.95	0.715	1.60	1.645	2.70	+0.42
5.40π	0.983	9.82	6.80	0.693	1.67	1.700	2.89	+0.30
5.45π	0.992	9.91	6.80	0.686	1.69	1.703	2.90	+0.17
$\theta_0 = 5.50\pi$	1.000	10.00	7.00	0.700	1.65	1.645	2.71	0.00
5.55π	1.010	10.10	6.80	0.673	1.73	1.713	2.94	−0.17
5.60π	1.020	10.20	6.80	0.667	1.75	1.715	2.95	−0.30
5.65π	1.029	10.29	6.95	0.676	1.72	1.673	2.80	−0.42
5.70π	1.038	10.38	7.35	0.709	1.62	1.560	2.44	−0.53
5.75π	1.046	10.46	8.10	0.775	1.40	1.340	1.80	−0.67
5.80π	1.055	10.55	9.45	0.895	0.95	0.900	0.81	−0.85

The results of this analysis are shown in Fig. 9. This illustration, in addition to giving detailed performance characteristics for the $3 + \frac{3}{4}$ mode, also indicates clearly the wealth of information which may be obtained from the complex admittance plane representation. Although the curves shown are self-explanatory, a few comments regarding their significance would seem to be in order. It is seen, for instance, that a coupling coefficient so adjusted that $(Qk)^2$ lies between 0.2 and 0.4 will produce a frequency range of essentially constant power. In particular, if we pick the curve for $(Qk)^2 = 0.4$ from the family of curves of Fig. 9(d), it will be seen that the variation in power over a bandwidth of $Q\delta = \pm 0.4$ is ± 2 per cent, while the corresponding value for the single resonator case, i.e., $(Qk)^2 = 0$, is minus 23 per cent. As the value of $(Qk)^2$ is increased beyond 0.4, the depression in the center of the mode becomes increasingly pronounced until it turns into a cusp for $(Qk)^2 = 1$. Mode shapes for $(Qk)^2 > 1$, though of no direct interest to this investigation, are indicated in Fig. 10 since they may be encountered in practice in cases of excessively tight coupling and could then be recognized as such. If the mode is traversed in the direction of increasing $|V_R|$ (or increasing frequency), such that the intersection of the electronic

admittance vector with the load line moves down along the latter as indicated by the arrows in Fig. 10(a), power changes smoothly until the Y_e-vector becomes tangent with the loop at 4. At this point there occurs a discontinuous jump in both power and frequency caused by the sudden shortening of the Y_e-vector from 4 to 7. From here on, power and frequency again become single valued functions of V_R. The mode shape corresponding to this uni-directional sweep is shown in Fig. 10(b). If the mode is traversed in the opposite sense we again encounter this discontinuity although it will now occur on the opposite side of the loop and, therefore, at a different repeller voltage and frequency. Fig.

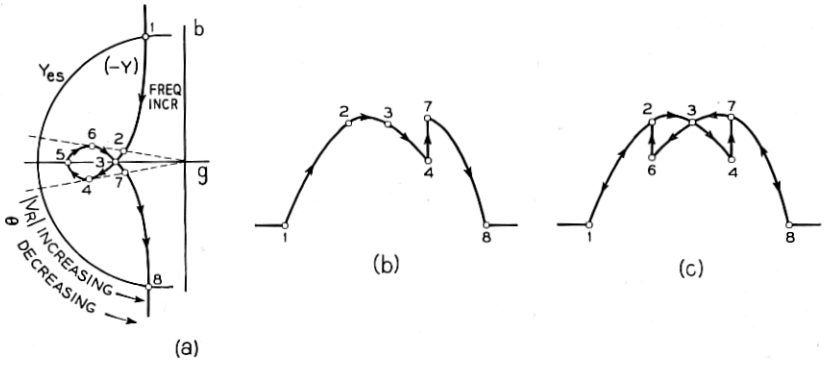

Fig. 10 — Production of load hysteresis by overcoupled cavities. (a) Load line for overcoupled cavities. (b) Oscillographic mode representation for unidirectional (sawtooth) repeller sweep. (c) Oscillographic mode representation for sinusoidal repeller sweep.

10(c) shows the load hysteresis effect as one might expect to observe it on the oscilloscope screen with a sinusoidal sweep applied to the repeller.

3.3 *Driving Point Properties of Two Coupled Resonators Having Unequal Q's*

The presentation of the theory of the coupled resonator reflex klystron will now be concluded by a discussion of the more general and, as we shall see, more useful case of two coupled cavities of unequal Q's. Specifically, we are considering the equivalent circuit shown in Fig. 11. By making approximations similar to those which led to equation 3.2, the input admittance for the case of unequal Q's may be derived as,[2, 4, 5]

$$\frac{Y}{G} = \left[1 + \frac{k^2 Q Q_s}{1 + (2Q_s\delta)^2}\right] + j2Q\delta\left[1 - \frac{(Q_s k)^2}{1 + (2Q_s\delta)^2}\right], \qquad (3.11)$$

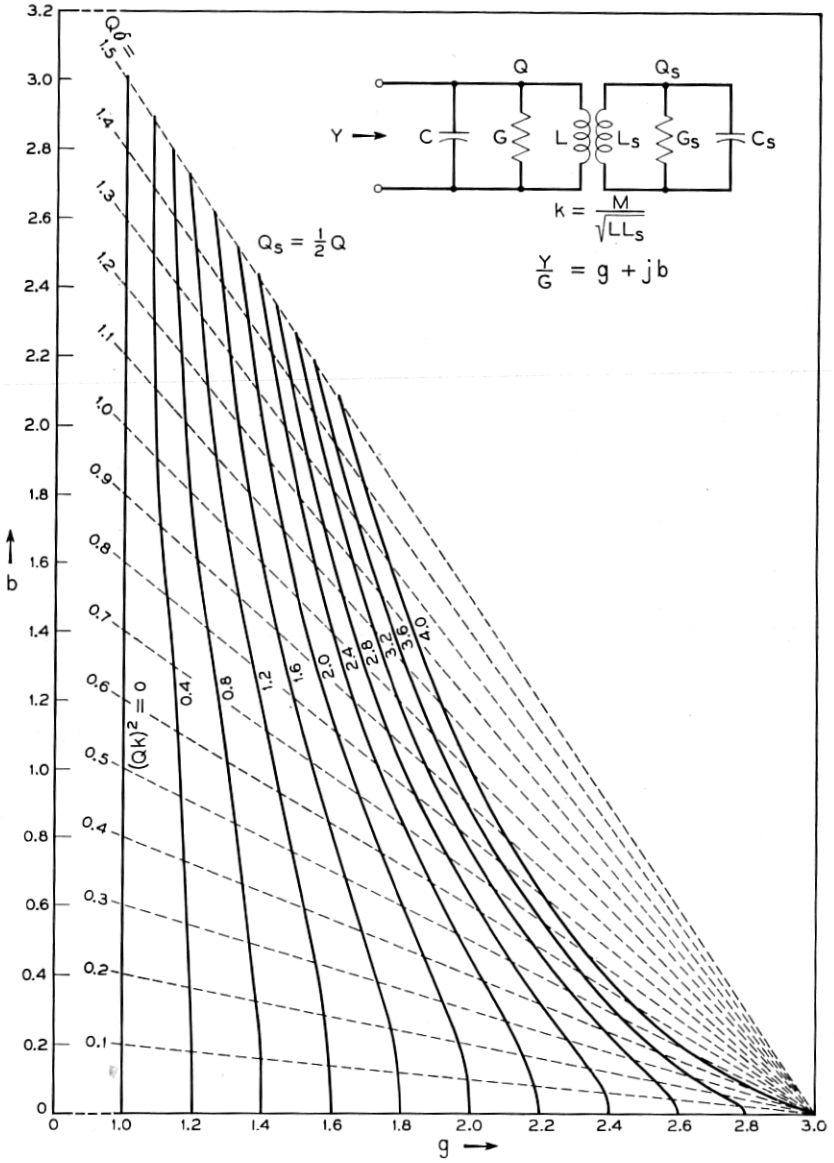

Fig. 11 — Driving point properties of two coupled, synchronously tuned resonators for the case of the secondary Q equal to half the primary Q.

or in more convenient form as,

$$\frac{Y}{G} = \left[1 + \frac{p(Qk)^2}{1 + p^2(2Q\delta)^2}\right] + j(2Q\delta)\left[1 - \frac{p^2(Qk)^2}{1 + p^2(2Q\delta)^2}\right], \quad (3.12)$$

where

$$p = \frac{Q_s}{Q}.$$

The above expression contains four variables, namely Y/G, (Qk), $(2Q\delta)$ and p, so that the complex admittance plane representation will now have to be restricted to particular values of p. One such plot, for $p = \frac{1}{2}$, appears in Fig. 11. It is similar to that of Fig. 7 except that only the positive half has been shown since equation (3.12) is symmetrical about the conductance axis; in addition, the parameter, $(Qk)^2$, has been carried to the point of critical coupling only, i.e., the formation of a cusp, and not beyond. The frequency contours are again seen to be straight lines crossing the horizontal axis at a value of conductance equal to the input conductance for the condition of critical coupling and $2Q\delta = 0$.

Equation (3.12) shows that the susceptance term will be zero for

(a) $$2Q\delta = 0,$$

or for

(b) $$p^2(Qk)^2 = 1 + p^2(2Q\delta)^2. \quad (3.13)$$

The value of conductance corresponding to condition (a) is given by $g = 1 + p(Qk)^2$ and the value corresponding to condition (b) by $g = 1 + 1/p$. It is interesting to note that this latter value which determines the point of intersection of the frequency contours, as well as of the admittance plot for critical coupling, with the conductance axis, is independent of the actual values of Q and the degree of coupling and only dependent upon p, the ratio of Q's. Thus in Fig. 11, which constitutes a plot for $p = 0.5$, the value of conductance at which all the above named contours meet is given by $g = 1 + 1/0.5 = 3$.

From what has been said before we know that at critical coupling the admittance locus forms a cusp intersecting the conductance axis at $g = 1 + 1/p$ at the frequency, $2Q\delta = 0$. Substituting this value of $2Q\delta$ into the conductance term of equation 3.12 and equating to $1 + 1/p$ yields

$$1 + p(Qk)^2 = 1 + \frac{1}{p}.$$

Hence

$$pQk = Q_s k = 1 \text{ (for critical coupling).} \tag{3.14}$$

The effect of reducing the secondary resonator Q is to broaden the frequency range over which a high input impedance or low admittance may be maintained. This is clearly illustrated in Fig. 12 where curves having the same value of conductance at resonance have been selected from Figs. 7 and 11 and superimposed to facilitate comparison.

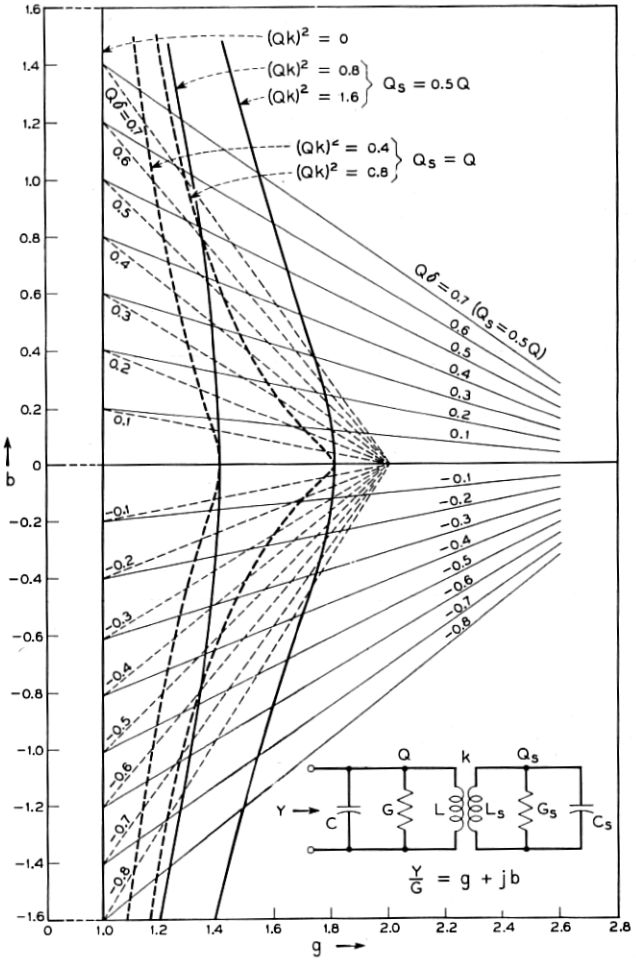

Fig. 12 — Comparison of admittance loci for coupled resonators of equal Q's with the case in which the secondary Q equals half the primary Q.

3.4 *Mode Shapes Obtainable with Two Coupled Resonators of Unequal Q's*

The complex admittance plane representation for the case of the secondary Q equal to half the primary Q is shown in Fig. 13(a) and the resulting mode shapes for the $3 + \frac{3}{4}$ repeller mode in Figs. 13(b), (c), (d), and (e). Again we notice that the coupling coefficient required for best modulation linearity is considerably smaller than that which results in a flat topped power curve. From Fig. 13(c) the most linear frequency-repeller voltage curve is associated with $(Qk)^2 \cong 0.8$ while from Fig. 13(d) a flat power mode may be obtained with a value of $(Qk)^2$ somewhat less than 1.6. In cases where neither modulation linearity nor constant power output are of importance but where the application requires a wide electronic tuning range, Fig. 13(e) shows the advantage to be gained from coupled cavities. Here, power output has been normalized with respect to its peak value within the particular mode under consideration and plotted against $Q\delta$. The ratio of half-power bandwidths for the curve corresponding to $(Qk)^2 = 2.4$ to the single resonator case, i.e., $(Qk)^2 = 0$, is seen to equal 1.73.

A phenomenon which may be encountered in the operation of the coupled resonator reflex klystron is illustrated by the $(Qk)^2 = 4.0$ curve of Fig. 13(b). Here we are dealing with a split mode in which the power, though everywhere a single valued function of repeller voltage, drops to zero over a range of repeller voltages centered about the middle of the mode. The reason for this behavior may be readily understood from an inspection of the complex admittance plane representation of Fig. 13(a). It is caused by the Y_{ss}-locus for the $3 + \frac{3}{4}$ repeller mode crossing the appropriate load line and thereby resulting in a frequency band over which the condition for oscillation cannot be met.

4.0 AN EXPERIMENTAL COUPLED-RESONATOR REFLEX KLYSTRON

The reduction to practice of the theoretical results obtained in the above study raises these requirements:

(1) An arrangement must be found which allows the coupling between primary and secondary cavities as well as between primary cavity and waveguide output line to be varied continuously and independently.

(2) Either primary or secondary resonators (or both) must be tunable to allow frequency adjustments for synchronous operation.

(3) Secondary resonator Q should be continuously variable.

(4) The secondary resonator should be detachable for independent determination of Q.

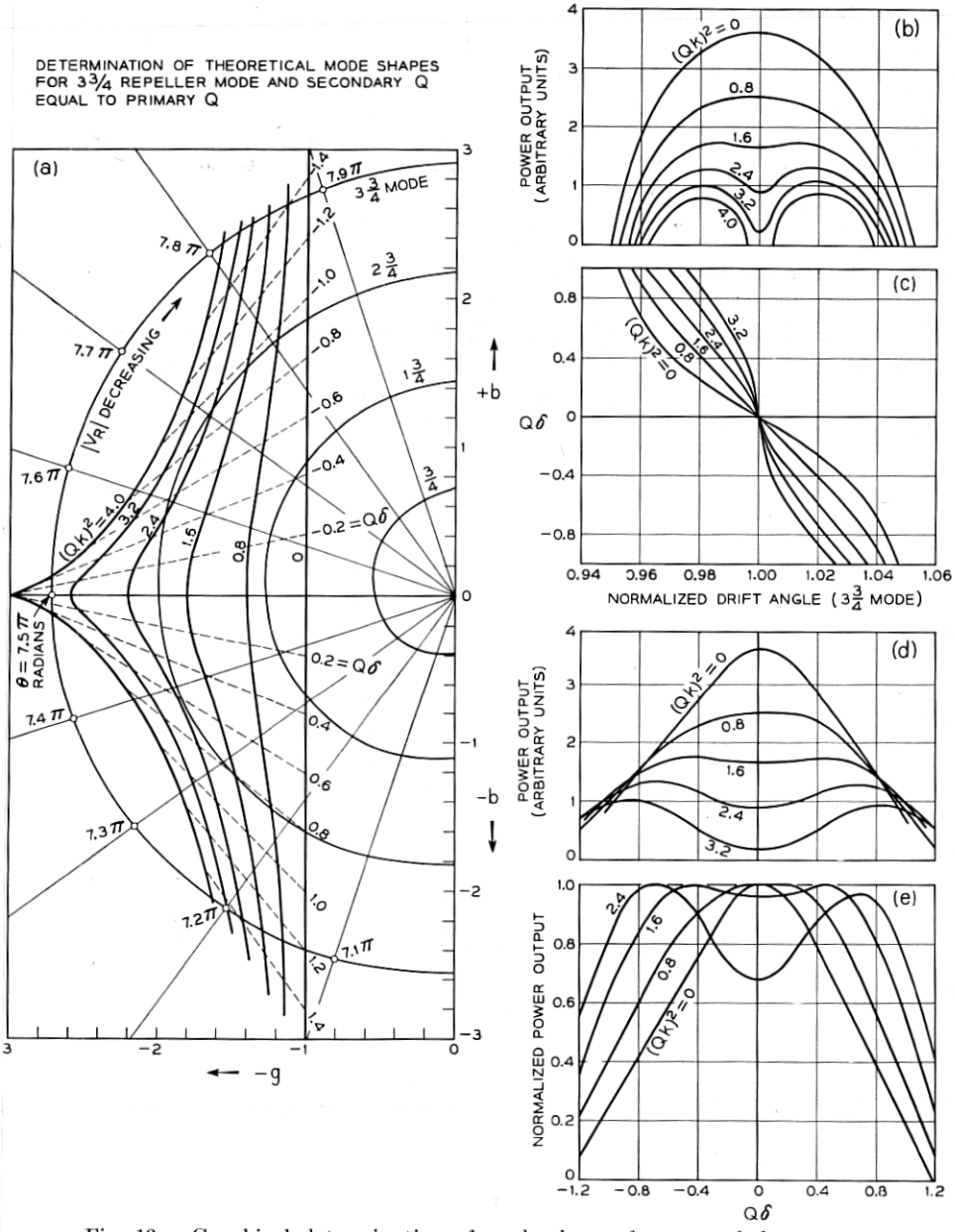

Fig. 13 — Graphical determination of mode shapes for a coupled resonator reflex klystron having the secondary cavity Q equal to half the primary Q. The effect of lowering the secondary Q may be studied by comparing the above curves with the corresponding ones shown in Fig. 9.

(5) Frequency at which these experiments are to be performed should be in a microwave band where good waveguide components and measurement techniques are available.

These considerations have led to the adoption of an external cavity type reflex klystron, the Sylvania 6BL6, as a vehicle for the experimental studies to be described, and operation in the 3700–4200 mc band.

4.1 *Constructional Features of Experimental Tube and Circuit*

The 6BL6 is one of a group of Sylvania low-voltage reflex klystrons[10] designed for use with external cavity resonators. Electrical connection to the interaction-gap grids is made through gold plated contact rings, formed from the disc seals which pass through the glass. The top ring is slightly smaller in diameter than the bottom ring, thereby permitting the insertion of the tube without disturbance to the associated cavity. Fig. 14 shows the external appearance of this tube and also contains a view of the major components of the passive circuit with cutouts to indicate the internal construction.

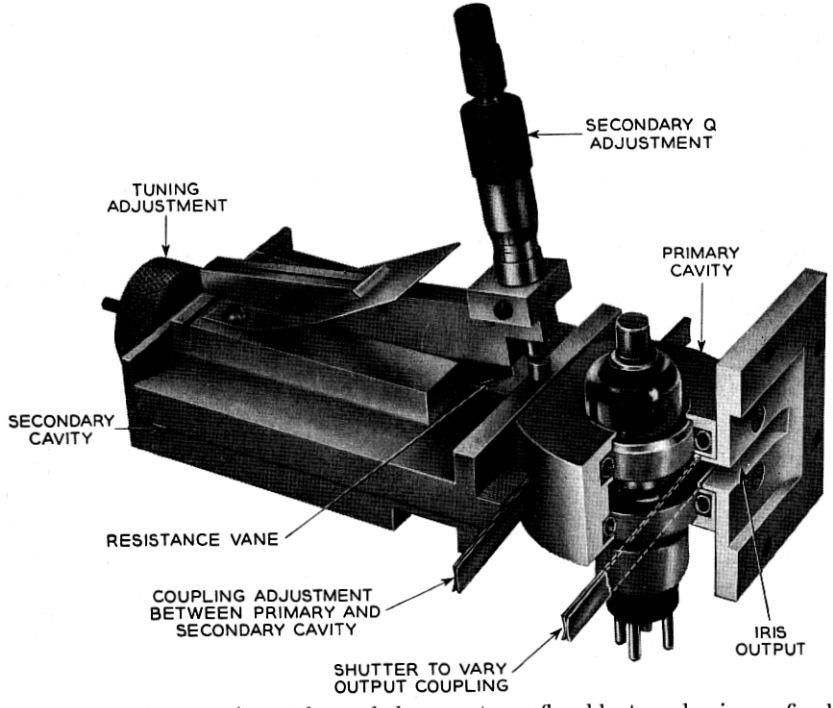

Fig. 14 — An experimental coupled resonator reflex klystron having a fixed frequency primary cavity.

Operation in the 4000-mc band was found to require a closely fitting primary cavity resonating in its principal mode. This unit, made of gold plated brass, is coupled to the output waveguide and secondary cavity respectively through two rectangular irises the sizes of which are independently variable by means of shutters. Toroidal contact springs located in circular grooves grip the inserted tube and complete the external circuit. The secondary cavity consists of a length of rectangular waveguide and uses a movable contacting plunger for tuning. A micrometer driven resistance vane may be inserted into this cavity through a longitudinal slot in its top surface thereby obtaining a wide range of continuously variable Q's. The entire unit is attached to the output waveguide by means of the adapter plate shown to the right of the primary cavity in Fig. 14.

A coupled resonator circuit having a tunable primary cavity is shown in the photograph of Fig. 15. The secondary cavity of this unit is identical to the one shown in the Fig. 14 but the primary resonator has been

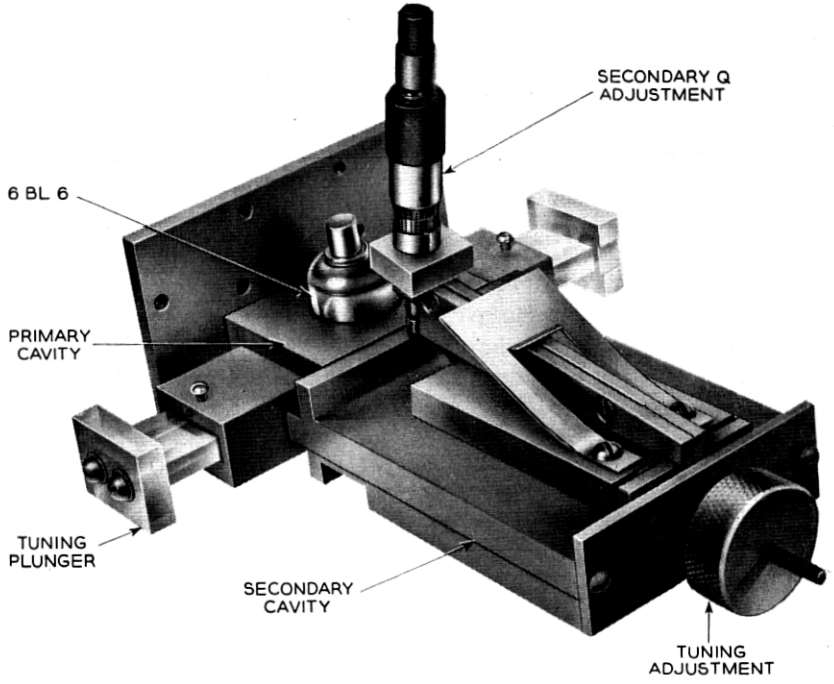

Fig. 15 — An experimental coupled resonator reflex klystron with a tunable primary cavity. The mechanical tuning range of this tube extends from 3700–4200 mc.

modified to take two non-contacting tuning plungers so dimensioned that they can be moved in very close to the glass wall of the 6BL6. In this way an operating frequency range from 3700–4200 mc was obtained.

4.2 *Qualitative Verification of Theory*

The results of a qualitative verification of the coupled-resonator reflex klystron theory are given in the form of oscillographic displays in Fig. 16. Photograph (a) shows the $(3 + \frac{3}{4})$-repeller mode of the 6BL6 with the secondary cavity completely decoupled. In photograph (b) the coupling iris and secondary Q have been adjusted for a flat topped output curve. The bandwidth of this curve for a variation in power output of ± 0.1 db was found to be 58 mc, i.e., considerably greater than the half-power bandwidth of the single resonator case above. Increasing $Q_s k$ beyond this point by either enlarging the coupling iris or withdrawing the resistance vane from the secondary resonator or a combination of both brings about the condition of critical coupling, illustrated by photograph (c). As explained earlier, this mode-shape results from the admittance plot of the passive circuit forming a cusp in the g-b plane. Comparison between this photograph and the theoretical mode of Fig. 9(b) for $(Qk)^2 = 1$ indicates good qualitative agreement. Coupling the secondary cavity still tighter, i.e., making the value of $Q_s k$ greater than unity, causes the formation of a loop in the circuit admittance plot and the consequent load hysteresis shown in photograph (d). Whereas all oscillograms discussed to this point have been obtained with a 60-cycle sinusoidal sweep applied to the repeller, the last one in this group, (e), results from a unidirectional (sawtooth) repeller sweep. The nature of this hysteresis effect has been explained earlier, and oscillograms one might expect to observe with overcoupled resonators for both sinusoidal and unidirectional sweeps were shown in Fig. 10. Again we note good qualitative agreement.

4.3 *Quantitative Verification of Theory*

As further strengthening of the theory underlying the operation of the coupled resonator reflex klystron a quantitative, experimental verification was undertaken. The methods used in connection with this work and the results obtained will form the subject of the sections to follow. To anticipate some of the conclusions which will be presented in the course of this description, let it be said here that the quantitative agreement between theory and experiment was found to be of an order high enough to justify amply the approximations involved in the ex-

pressions for both electronic admittance and passive circuit admittance, and to establish confidence in the method of analysis proposed to predict tube performance under a variety of conditions.

Since theoretical results had been worked out for the cases of the secondary Q equal to the primary Q and for the secondary Q equal to

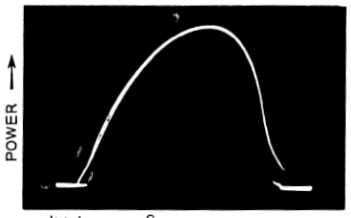

(a)

SECONDARY RESONATOR COMPLETELY DECOUPLED. HALF POWER ELECTRONIC TUNING RANGE EQUAL TO 49 MC.
(PEAK POWER = 100 MW)

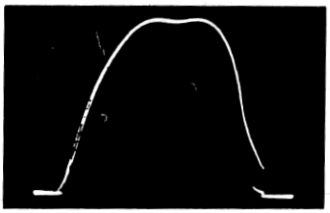

(b)

SECONDARY RESONATOR COUPLING AND Q ADJUSTED FOR FLAT TOPPED MODE SHAPE. BANDWIDTH FOR POWER VARIATION OF ± 0.1 DB IS 59 MC.

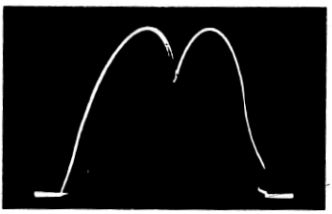

(c)

MODE SHAPE FOR CONDITION OF CRITICAL COUPLING, i.e., $Q_SK = 1$

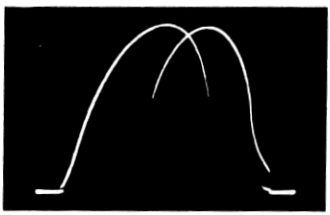

(d)

LOAD HYSTERESIS DUE TO OVERCOUPLING, i.e., $Q_SK > 1$

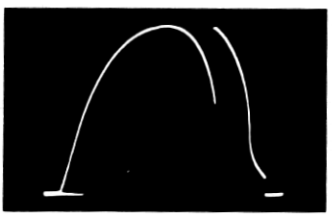

(e)

SAME AS (d) EXCEPT FOR UNIDIRECTIONAL (SAWTOOTH) REPELLER SWEEP

Fig. 16 — Qualitative verification of theory. These oscillograms were obtained with a 6BL6 in the circuit of Fig. 14 and the following operating conditions: $V_0 = 325V$, $I_k = 28$ ma, $f_0 = 3800$ mc, $3 + \frac{3}{4}$ cycle repeller mode.

half the primary one, (see Figs. 7 and 11, respectively) it was decided to establish the same conditions in the experimental tube and to compare the results thus obtained with those predicted by theory.

Prerequisites for the execution of these experiments were:

(a) Knowledge of the primary Q.

(b) Complete calibration of the secondary cavity with respect to both the variation of Q_s with penetration of resistance vane and variation of coupling coefficient with size of coupling iris.

(c) Knowledge of the location of the load lines with respect to the small signal electronic admittance plot in the complex admittance plane.

4.3.1 *Determination of Primary Q.* The above parameter is understood to denote the "operating" or loaded Q of the tube with the output iris adjusted to its final and permanent size and the secondary cavity completely decoupled. For the case of an inductively tuned (fixed gap) reflex klystron, it may be determined experimentally using the expression,[7]

$$Q = \pi f_0^2 \left| \frac{\frac{d\tau}{dV_R}}{\frac{df}{dV_R}} \right|_{f\tau=N+3/4} - \pi(N + \tfrac{3}{4}), \tag{4.1}$$

where τ denotes the repeller space transit time. Both $d\tau/dV_R$ and df/dV_R are to be evaluated at the center of the mode.

The functional relationship between τ and V_R was obtained by placing the 6BL6 in the tunable primary cavity of Fig. 15 and determining the repeller voltage for maximum power output over the mechanical tuning range of the cavity. Since the same repeller mode was used throughout this test, τ must also have been the same at each of these frequencies, namely equal to $(N + \frac{3}{4})/f$ seconds. The experimentally determined plot of repeller voltage vs. frequency is given in Fig. 17. It is seen to be a straight line described by the equation,

$$f = (13.5V_R + 2495) \text{ mc} \tag{4.2}$$

and since, for the $3 + \frac{3}{4}$-repeller mode,

$$\tau = \frac{3.75}{f_{(\text{mc})}} 10^{-6} \text{ sec.}, \tag{4.3}$$

the desired relation between τ and V_R is obtained from the above two equations as

$$\tau = (3.6V_R + 665)^{-1} \text{ sec.}, \tag{4.4}$$

whence the numerator of equation 4.1 follows as

$$\left|\frac{d\tau}{dV_R}\right| = \frac{3.6}{(3.6V_R + 665)^2}\ 10^{-6}\ \text{sec/volt.} \tag{4.5}$$

It remained only to replace the 6BL6 in the fixed tuned primary cavity, in which all subsequent tests were performed, and to determine the midmode repeller voltage and frequency. These values were found to be 96 volts and 3800 mc respectively, thus yielding by substitution into equation (4.5),

$$\left|\frac{d\tau}{dV_R}\right| = \frac{3.6 \times 10^{-6}}{(3.6 \times 96 + 665)^2} = 3.52 \times 10^{-12}\ \text{sec/volt.}$$

The demoninator of equation (4.1) simply denotes the "modulation sensitivity" at the center of the mode. A simple measurement estab-

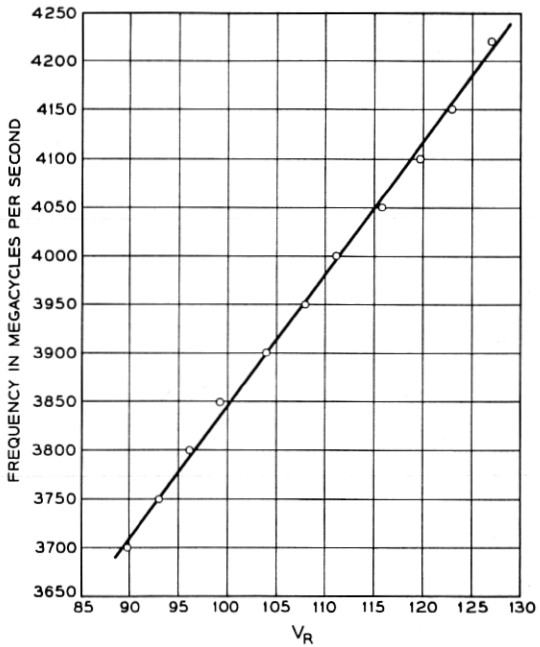

Fig. 17 — Experimental determination of the relation between frequency and repeller voltage. Points shown were obtained with a 6BL6 in tunable primary cavity of Fig. 14 with secondary cavity completely decoupled and operation in the 3 + ¾ repeller mode at a beam voltage, $V_0 = 325V$. Frequency was varied by means of tuning plungers and repeller voltage recorded for maximum power output. Relation is given by, $f = (13.5V_R + 2495)$ mc.

lished its value as,

$$\left| \frac{df}{dV_R} \right| = 1.12 \text{ mc/volt.}$$

Substitution into equation (4.2) then gave the value of primary Q as,

$$Q = \pi(3.8)^2 10^{18} \frac{(3.52)10^{-12}}{(1.12)10^6} - \pi(3.75) = 130.$$

The entire Q-determination, incidentally, as outlined above, was repeated for the $2 + \frac{3}{4}$ mode and resulted in $Q = 128.8$ thus affording an excellent and independent double check.

4.3.2 *Calibration of Secondary Resonator.* To facilitate the establishment of controlled and reproducible conditions of secondary Q and coupling coefficient, two calibration curves had to be obtained. One, relating the values of secondary Q with the readings of the micrometer controlling the depth of insertion of the resistance vane and the other, relating the coefficient of coupling, k, with the coupling iris width. The latter could be varied by means of gold plated spring shutters as shown in Figs. 14 and 15.

This calibration of the secondary cavity was carried out in three distinct phases. The first phase involved the determination of the variation of Q_s with micrometer setting for values of Q_s ranging from 500 to 2000. The second phase, which was based on the results obtained in phase one, yielded the complete calibration of the coupling iris and the third and last phase, in turn dependent on results of phase two, yielded values of Q_s down to 65. The reasons for this particular sequence of measurements will become apparent in the following more detailed description.

By means of a Q-measurement technique[8] based on an oscillographic display of reflected power, points on the calibration curve were obtained as indicated by the circles in Fig. 18. It is seen that the lowest value of Q_s which could be determined by this method was 550. For lower values of Q, the sweep range of the signal generator became insufficient to display the required fraction of the resonance curve; in addition, the cavity proved excessively undercoupled to permit reliable measurements of bandwidths.

Using the values of Q_s thus determined and a particular property of coupled resonators covered earlier in this text and further elaborated below, the relation between coupling coefficient and iris width was established. It was shown earlier that an overcoupled secondary cavity gives rise to load hysteresis manifesting itself in mode shapes as sketched

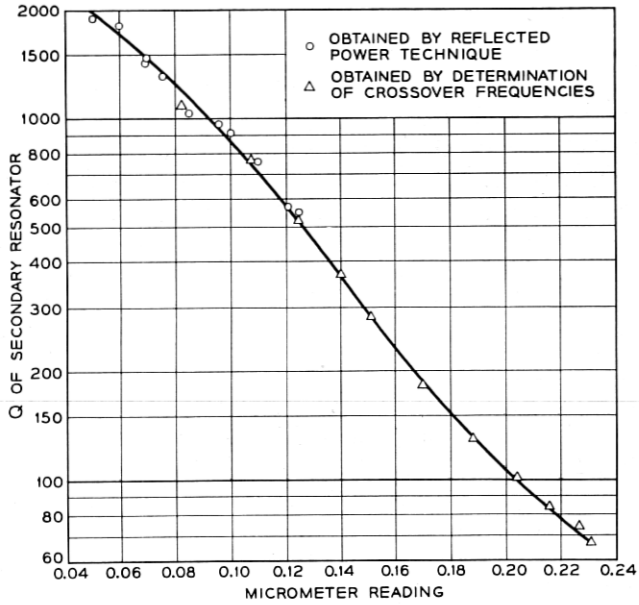

Fig. 18 — Calibration of secondary cavity. Variation of secondary Q with reading of micrometer controlling depth of insertion of resistance vane.

in Fig. 10 and shown in the form of an oscilloscope pattern in Fig. 16(d). Conditions pertaining at the crossover point were described by equation (3.13), which stated:

$$p^2(Qk)^2 = 1 + p^2(2Q\delta)^2,$$

or, since $pQ = Q_s$

$$(Q_s k)^2 = 1 + (2Q_s\delta)^2.$$

Hence the two frequencies corresponding to the crossover point are given by

$$\delta_{1,2} = \pm \frac{1}{2}\sqrt{k^2 - \left(\frac{1}{Q_s}\right)^2} \tag{4.6}$$

and their difference, $\Delta\delta$, by

$$\Delta\delta = \sqrt{k^2 - \left(\frac{1}{Q_s}\right)^2}. \tag{4.7}$$

Equation (4.7)[4, 5] provides an experimental method of determining k since $\Delta\delta$ can be accurately measured and Q_s is known from previous tests.

The actual procedure adopted in calibrating the coupling iris was this: The secondary cavity was set to a fairly high and known value of Q_s, say 1500, and the coupling iris adjusted to the smallest width which still resulted in overcoupling, i.e. in $Q_s k > 1$, and thus displayed the desired load hysteresis on the oscilloscope screen. By means of a high-Q absorption wavemeter the crossover frequencies were determined and, along with the known value of Q, substituted into equation (4.7) which then yielded the value of k. As a double check the above procedure was repeated for several values of Q_s and in accordance with theory the coupling coefficient, k, found to be a function only of the iris coupling width. A typical set of readings is given in Table II. They show that though Q_s was varied by a ratio of nearly 3:1, the resulting values of k only differed by about one-half per cent. Measurements as shown in the table were repeated for various iris widths. They resulted in the curve of Fig. 19.

To complete the calibration of the secondary cavity it was necessary to extend the relation between Q_s and micrometer readings to values lower than could be obtained by the reflected power technique. This was carried out with the aid of Fig. 19 in the following manner: With the coupling iris adjusted to its maximum width of 0.5″, the secondary Q was varied until the condition of critical coupling, as observed by the formation of a cusp on the oscilloscope pattern (see Fig. 16(c)), was reached. Since this condition is characterized by $Q_s k = 1$ and since the value of k corresponding to the iris opening could be read off the curve of Fig. 19, the value of Q_s then followed simply as the reciprocal of k. This measurement was repeated for successively smaller iris openings and the points shown as triangles in Fig. 18 were obtained. Inspection of this figure also reveals that these values of Q_s, ranging from 65 to 1100, overlap and coincide with values of Q_s determined

TABLE II

Coupling Iris Width (inches)	Secondary Cavity Q, Q_s	Crossover Frequencies f_1 and f_2 (mc)	$\Delta f = (f_1 - f_2)$ (mc)	$\delta = \frac{2\Delta f}{f_1 + f_2}$	From Equation (4.7), $k = \frac{1}{\sqrt{(\Delta\delta)^2 + (1/Q_s)^2}}$
0.500	1430	3749.9 3694.4	55.5	14.92×10^{-3}	14.93×10^{-3}
0.500	975	3748.4 3693.1	55.3	14.90×10^{-3}	14.90×10^{-3}
0.500	573	3745.2 3690.4	54.8	14.74×10^{-3}	14.85×10^{-3}

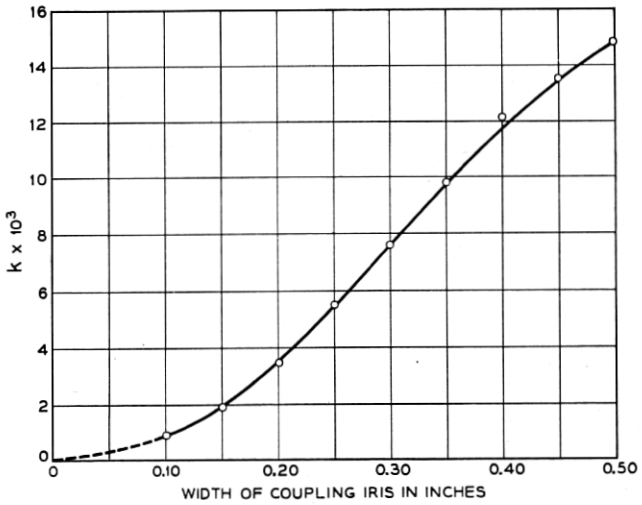

Fig. 19 — Calibration of coupling iris. Variation of coupling coefficient with width of coupling iris.

independently by the reflected power method. The significance of this experimental agreement is twofold. It serves to prove the correctness of the calibration curves of Figs. 18 and 19 and beyond that may be regarded as verifying much of the theory of the coupled resonator reflex klystron.

4.3.3 *Comparison of Experimental and Theoretical Mode Shapes.* Knowing the primary (operating) Q and the calibration of the secondary resonator, controlled operating conditions were established and the experimental mode shapes shown in the left hand column of Fig. 20 obtained. The first three families of curves in this column are the results of point by point measurements in which repeller voltage, taken as the independent variable, was varied by known amounts about its midmode value and the corresponding values of RF power output and frequency were determined by a thermistor-bridge-wattmeter and high-Q wavemeter respectively. The last family of curves in this group, (d), is derived from (c); in it power has been normalized with respect to its maximum value within the mode thus permitting the convenient determination of midmode percentage reduction of power and electronic tuning range to any desired power level for various values of $(Qk)^2$.

Additional details of the test conditions which gave rise to the ex-

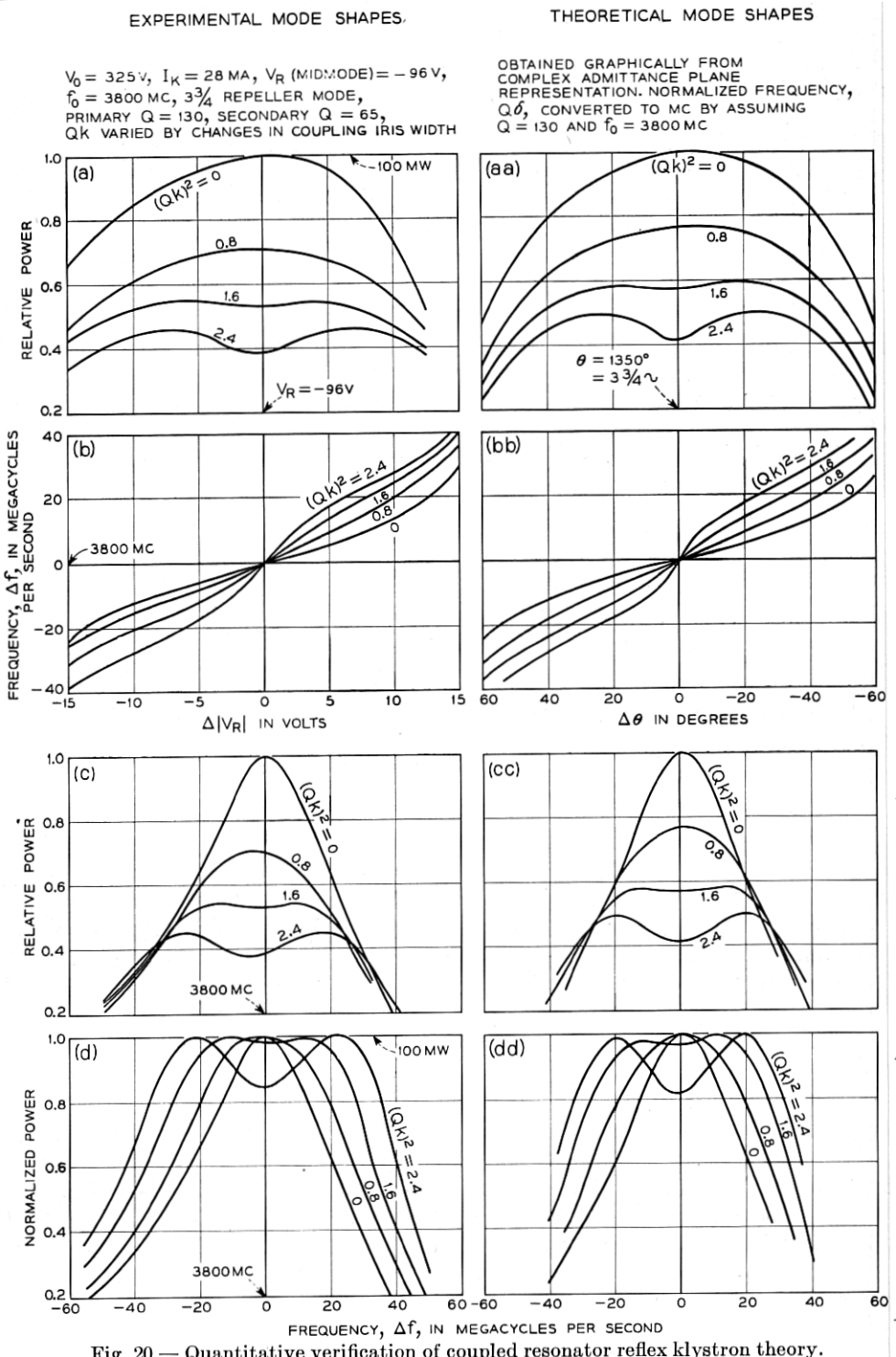

Fig. 20 — Quantitative verification of coupled resonator reflex klystron theory. Curves (a) and (b) were obtained experimentally by changing the repeller voltage about its midmode value and noting the corresponding values of power and frequency. Curves (c) and (d) were deduced from (a) and (b). The theoretical curves were obtained graphically from a complex admittance plane plot similar to those of Figs. 9 and 13.

perimental curves shown are as follows:

6BL6 repeller mode = $3 + \frac{3}{4}$ cycles
Resonator voltage, V_0 = 325 volts
Cathode current, I_k = 28 ma
Midmode repeller voltage, V_R = −96 volts
Midmode frequency, f_0 = 3800 mc
Secondary Q, Q_s = ½ primary Q = 65, obtained by micrometer reading of 0.234 (see Fig. 18)

The parameter, $(Qk)^2$, was varied by adjusting the iris width, and hence k, according to Table III.

A few words, next, about the method by which the theoretical curves of Fig. 20 were derived. Input admittance plots for two coupled resonators having $Q_s = \frac{1}{2}Q$ were given earlier in this report (see Fig. 11).

TABLE III

$(Qk)^2$	k (for Q = 130)	Iris width from Fig. 19 in inches
0.0	0.00	0.000
0.8	6.88×10^{-3}	0.285
1.6	9.73×10^{-3}	0.350
2.4	11.90×10^{-3}	0.405

These included graphs for the values of $(Qk)^2$ listed in Table III and thus of direct use in a graphical admittance plane analysis such as described in Section 3.2. To establish correlation, however, between theory and experiment, it was necessary to determine the location of the load lines in relation to the small-signal electronic admittance plot for the $3 + \frac{3}{4}$ repeller mode. This was performed graphically by trial and error as follows: a number of electronic admittance loci were drawn and their interactions with the load line for $(Qk)^2 = 2.4$ studied. In particular, the ratio of minimum to maximum power was calculated for each trial until one was found agreeing well with the experimental value of 0.845 (see Fig. 20d). This latter trial, then, was taken as representing the proper relation between electronic and circuit admittance. Mode plots for other values of $(Qk)^2$ were determined without further reference to the experimental results and allowed to fall where they may.

In comparing the theoretical and experimental curves, then, the following points should be kept in mind: the frequency scales of the theoretical curves are normally expressed in terms of $Q\delta$. This was converted

to megacycles in Fig. 20 by using the relation,

$$\Delta f = (Q\delta)\frac{f_0}{Q}\text{ mc},$$

where Q was found to equal 130 by the independent measurement described in section 4.3.1 and f_0 taken as 3800 mc. The vertical power scales of the theoretical curves are not entirely independent of the experimental plots in as much as one of the latter, namely the plot for $(Qk)^2 = 2.4$, was used in determining the location of the load lines within the spiral diagram.

The curves presented in Fig. 20 are largely self-explaining. They indicate good agreement between theory and experiment. What disagreement there is, may be traced primarily to the assumptions involved in the small signal klystron theory not being fully met in practice. Thus, the slight discrepancy between Figs. 20(a) and (aa) may be due to the drift angle not being linearly related to repeller voltage or possibly due to the phase angle of the electronic admittance being affected by the magnitude of the gap voltage.[11] These factors, however, are eliminated in the mode plots (c) and (d), which for this reason exhibit better mode symmetry and very close agreement with theory.

4.4 *Performance Data*

The experimental curves of Fig. 20 were obtained with particular values of $(Qk)^2$ and Q_s/Q for which the input admittance of two coupled resonators had been computed and plotted earlier. As pointed out before, these values were chosen merely because they facilitated comparison between theory and experiment; they were not to be regarded, however, as representing optimum conditions. Whereas these curves had been obtained for a fixed secondary Q (namely equal to half the primary one), with changes in coupling-iris width producing the desired variations in $(Qk)^2$, the demonstration of optimum performance which follows was pursued along different lines. Here, the coupling iris was opened to its maximum width (0.500″) and the secondary Q adjusted until the conditions shown by the oscillograms of Fig. 21 were obtained.* These oscillograms indicate a number of mode shapes useful in applications requiring power output to be essentially independent of frequency. It is

* In adjusting the circuit parameters for a flat topped mode it should be borne in mind that the variation in power with frequency is a function of $Q_s k$ whereas the actual bandwidth varies inversely with Q_s. For a maximum flat band, therefore, Q_s should be chosen as small as possible consistent with a value of $(Q_s k)^2$ of about 0.35. In practice the lowest value of Q_s which can be used will be determined by the highest value of k obtainable with a given coupling iris.

seen that the useable bandwidth depends on the degree of flatness. Thus, if the application requires power to be absolutely constant, the useable bandwidth equals 39 mc; it increases to about 70 mc for a fluctuation in power of ±0.2 db. Fig. 21 also lists the values of half power electronic tuning for the oscillograms shown. They are seen to range between 107 and 113 mc.

By way of comparison, the mode shape for the case of a completely decoupled secondary resonator was shown in Fig. 16(a). Its peak power was found to equal about 100 mw, or about twice the power of the flat topped modes of Fig. 21, and its half power electronic range equaled 50

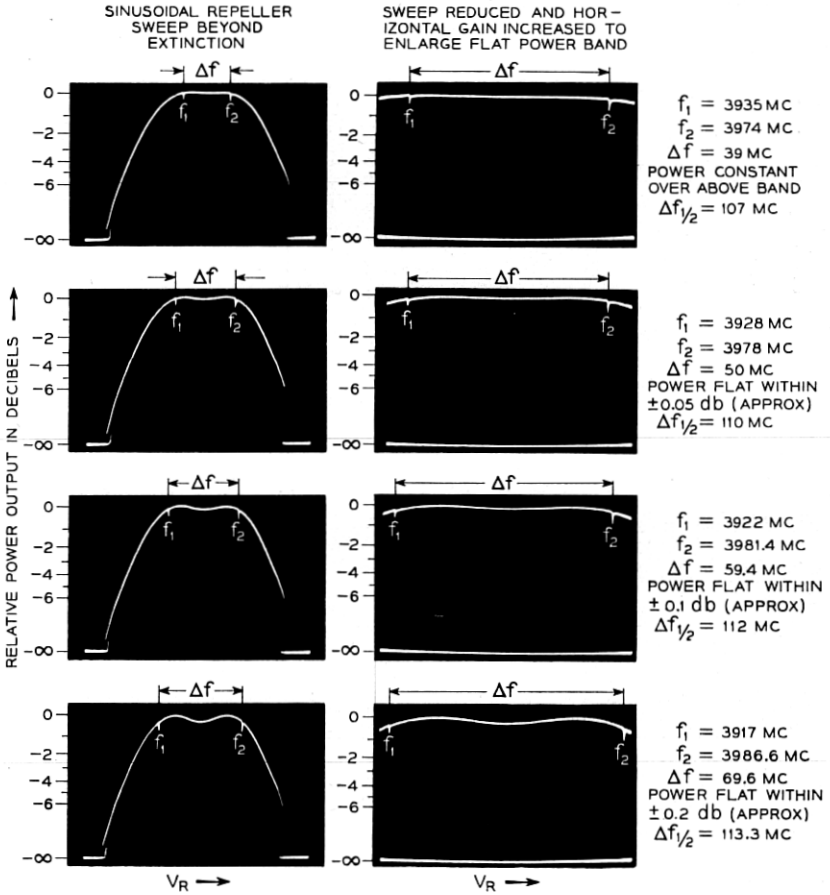

Fig. 21 — Oscillograms showing flat power bands obtainable with coupled resonator reflex klystron. 6BL6 operating in 3 + ¾ mode, $V_0 = 325$ V, $I_k = 28$ ma, zero DB power level corresponds to 50 milliwatts.

mc. The price, then, we must pay for a better than two fold increase in electronic tuning and for a frequency range of constant power is a 3 db loss in the available power output.

Using the tunable primary cavity shown in Fig. 15, the mode performance just described could be obtained about any center frequency between 3700 and 4200 mc.

5.0 APPLICATIONS OF THE COUPLED-RESONATOR REFLEX KLYSTRON

A numer of applications making use of the variety of mode shapes which may be obtained with the coupled resonator reflex klystron were indicated in the introductory section of this paper. Some of these applications were tried experimentally and are described below, others,

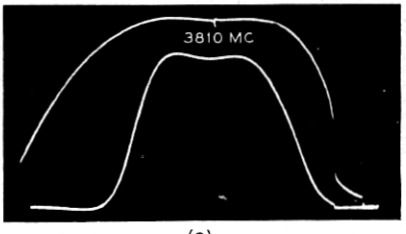

(a)

USE OF COUPLED-RESONATOR REFLEX KLYSTRON IN GAIN COMPARATOR TO DISPLAY BANDPASS CHARACTERISTIC OF MICROWAVE CHANNEL FILTER. TOP TRACE REPRESENTS INCIDENT POWER, LOWER TRACE TRANSMITTED POWER.

CENTER FREQUENCY OF FILTER = 3810 MC
PASS BAND = 28 MC

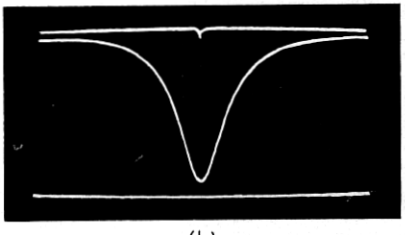

(b)

USE OF COUPLED-RESONATOR REFLEX KLYSTRON AS SWEPT FREQUENCY SOURCE IN DETERMINATION OF Q OF UNKNOWN RESONATOR BY REFLECTED POWER METHOD. TOP TRACE REPRESENTS POWER INCIDENT UPON CAVITY UNDER TEST, MIDDLE TRACE REFLECTED POWER AND LOWER TRACE ZERO POWER LEVEL. (NOTE FLATNESS OF INCIDENT POWER TRACE)

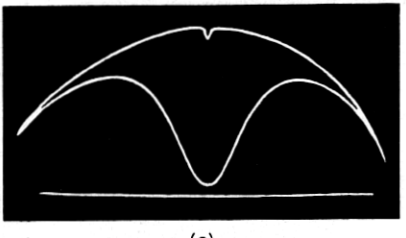

(c)

OSCILLOSCOPE DISPLAY FOR SAME RESONATOR RESULTING FROM USE OF CONVENTIONAL KLYSTRON AS SWEPT FREQUENCY SOURCE

Fig. 22 — Examples of application of coupled resonator reflex klystron as microwave sweeper.

and in particular those making use of the improved modulation linearity resulting from the use of two resonators, could not be tried since the required test apparatus[9] was unavailable. The close correlation between theory and experiment, however, as demonstrated in Section 4.3.3 leaves little doubt as to the feasibility of such applications.

Two examples of the use of the coupled resonator reflex klystron as a microwave sweeper are given in Fig. 22. The first example shows the band pass characteristic of a channel filter, 28 mc wide. The second example demonstrates the use of this tube in a Q-measurement scheme[8]

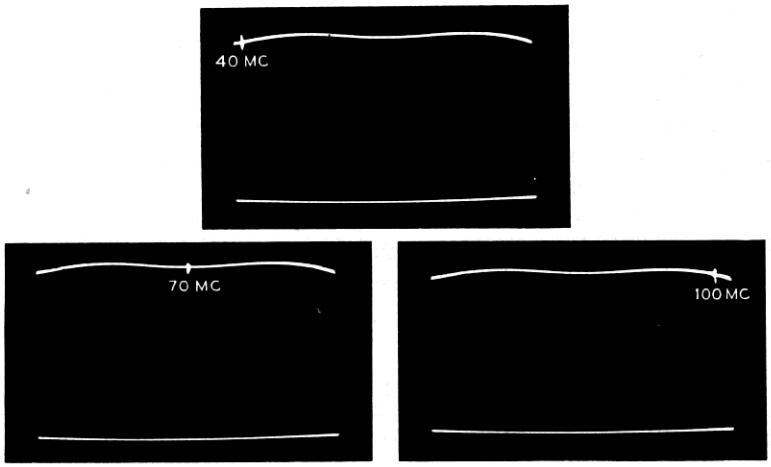

(a)

SUCCESSIVE PHOTOGRAPHS OF OSCILLOSCOPE DISPLAY SHOWING IF-POWER AS A FUNCTION OF FREQUENCY WITH SIGNAL GENERATOR TUNED TO DIFFERENT FREQUENCIES

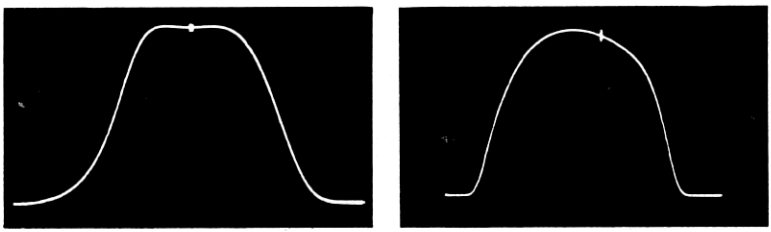

(b)

GAIN-FREQUENCY CHARACTERISTIC OF IF AMPLIFIER USING COUPLED-RESONATOR REFLEX KLYSTRON AS SWEEP SOURCE

CENTER FREQUENCY OF IF-AMPL = 70MC
FLAT BANDWIDTH OF IF-AMPL = 22MC

(c)

GAIN-FREQUENCY CHARACTERISTIC OF SAME IF AMPLIFIER AS OBTAINED BY CONVENTIONAL (SINGLE RESONATOR) REFLEX KLYSTRON. DISTORTION IN GAIN ENVELOPE DUE TO MODE SHAPE OF KLYSTRON.

Fig. 23 — Example of application of coupled resonator reflex klystron as intermediate frequency sweeper.

based on the oscillographic display of reflected power. The advantage of a flat-topped mode shape for this measurement may be seen by comparison with the oscillogram of Fig. 22(c) which was obtained for the same resonator under test using a conventional reflex klystron as swept frequency source.

The center frequency of the flat power band obtainable with the coupled resonator reflex klystron may be shifted into the intermediate frequency range by mixing its output with a suitable local oscillator. This is shown in Fig. 23 where the first three oscillograms represent a power band flat to within ± 0.1 db and 60 mc wide centered around an IF frequency of 70 mc. The frequency markers are obtained from a signal generator tuned to the frequencies indicated and coupled lightly to the output of the mixer. Fig. 23(b) shows the gain-frequency characteristic of a 70 mc-IF strip having a useful bandwidth of 22 mc. The last oscillogram shows the gain-frequency characteristic of the same IF amplifier with the coupled resonator reflex klystron replaced by one of conventional design. Due to the inadequate electronic tuning range of this klystron and due to the asymmetry of its mode shape, the gain envelope of the IF amplifier appears distorted.

6.0 CONCLUSIONS

The theory and reduction to practice of a coupled resonator reflex klystron have been presented. This device differs from the conventional reflex klystron in that the electronic admittance interacts with the input admittance of two coupled resonators. Significant and advantageous changes in performance resulting therefrom are:

(1) Power output can be made to be substantially flat over part of the electronic tuning range. The frequency range of flat power is greater than the half power electronic tuning range of a klystron having the same electron-optical system but interacting with a single resonator.

(2) The half-power electronic tuning range of the coupled resonator klystron is more than twice that of the equivalent single resonator klystron.

(3) Modulation linearity may be obtained over a greatly increased frequency swing.

A reduction in power output of about 3 db occurs for a secondary resonator Q and coupling coefficient adjustment designed to yield a maximum flat band or maximum electronic tuning, a much smaller reduction in output power, perhaps 10 per cent, will provide a substantial improvement in modulation linearity.

Qualitative and quantitative experimental verifications of the theory were undertaken and good agreement obtained. Oscillograms of mode shapes having a range of constant power output and wide half-power electronic tuning were presented together with a number of applications of the coupled resonator reflex klystron both as a microwave and as an intermediate frequency sweep source. Other applications were indicated and additional ones may suggest themselves to the reader.

It is believed that the addition of the second resonator makes the reflex klystron a more useful device in many of its more important applications.

ACKNOWLEDGEMENTS

The writer wishes to express his appreciation to J. O. McNally for the advice and encouragement received in the execution of this work. The assistance of the thesis advisor, Prof. John B. Russell of the Electrical Engineering Department of Columbia University, is also gratefully acknowledged.

REFERENCES

1. Pierce, J. R., and W. G. Shepherd, Reflex Oscillators. Bell System Tech. J., **26,** pp. 460–690, July, 1947. This reference constitutes a very complete treatment of reflex klystron theory and practice. The derivation of the expression for electronic admittance is given in Appendix III, pages 639–643; of particular interest to the coupled resonator reflex klystron is Pierce and Shepherd's treatment of Frequency Sensitive Loads and Long Lines Effects, pp. 523, where it is shown that certain load conditions encountered in the operation of reflex klystrons may result in load hysteresis similar to the one described in the preceding paper as due to an overcoupled secondary resonator.
2. Martin, R. A., and R. D. Teasdale, Input Admittance Characteristics of a Tuned Coupled Circuit. I. R. E., Proc., p. 57, January, 1952, and correction to this paper published in I. R. E., Proc., p. 459, April, 1952. This paper presents a precise expression for the input admittance of two coupled resonant circuits and gives plots of specific numerical examples. The expression for input admittance given in the above named correction reduces to equation (3.2) and (3.12).
3. Bleaney, B., Electronic Tuning of Reflection Klystrons. Wireless Engineer, p. 6, Jan., 1948. A valuable background paper on the mechanics and maximization of electronic tuning.
4. Very High-Frequency Techniques, Vol. II, Radio Research Laboratory, Harvard University. (McGraw-Hill). Chapter 31, p. 849 contains a concise and valuable treatment of reflex klystron theory. It leads up to the application of external-cavity reflex klystrons in wide tuning range coaxial resonators. In the course of explaining some load hysteresis phenomena which are sometimes caused in these circuits by parasitic resonances or excitation of undesired modes, a simplified expression for the input admittance of two coupled resonators is given. This expression is similar to equation (3.12). An experimental method is also suggested (p. 869) to measure the coupling coefficient between the main resonator and the undesired resonance. Use has been made of this method in the calibration of the secondary resonator in Section 4.3.2.

5. Spangenberg, K. R., Vacuum Tubes, p. 601. (McGraw-Hill). This reference covers essentially the same material as Reference 4.
6. Reference Data for Radio Engineers, Third Edition, p. 121, Federal Telephone and Telegraph Corp. Here a universal chart of the selectivity (transfer characteristic) of two coupled tuned circuits is presented. The format and choice of variables of this presentation has inspired the selection of the equivalent quantities applying to the driving point properties of coupled tuned circuits.
7. Harmen, W. W., and J. H. Tillotson, Beam-Loading Effects in Small Klystrons. I. R. E., Proc., p. 1419, Dec., 1949. Equation (3) of this reference is identical with equation (4.1) and has been used in the experimental determination of the primary operating Q.
8. Reed, E. D., A Sweep Frequency Method of Q Measurement for Single-Ended Resonators. Proc. National Electronics Conference, Vol. VII, p. 162. Also reprinted as Bell Telephone System Monograph 1953. This method of Q-measurement was used in the calibration of the secondary resonator described in Section 4.3.2. The coupled resonator reflex klystron provides a useful tool for this type of measurement as may be seen from Fig. 22(b).
9. Albersheim, W. J., Measurement Techniques for Broad-Band Long-Distance Radio Relay Systems. I.R.E., Proc., p. 548, May, 1952. Figs. 4(a) and 4(b) of this reference give the block diagram of a "Linearity-Test-Set" developed at Bell Telephone Laboratories to determine the modulation linearity of a reflex klystron used as FM-deviator.
10. Boehlke, P. G., and F. C. Breedan, External Cavity Klystron. Electronics, p. 114, July, 1947. This paper gives an account of the design considerations which led to the development of the 6BL6 reflex klystron. It also contains useful information on its performance characteristics.
11. Garrison, J. B., A Qualitative Analysis of Hysteresis in Reflex Oscillators. Radiation Laboratory Report No. 650, dated Feb. 4, 1946. In this treatment on the causes of electronic hysteresis Garrison shows (on page 5) that a dependence of the phase angle of the electronic admittance upon the magnitude of RF gap voltage will give rise to asymmetry in the mode plot of power output vs. repeller voltage although the power vs. frequency relation will be symmetrical. (Note that the experimental mode plots for $Qk = 0$ of Figs. 20(a) and (c) show evidence of the same phenomenon.)